AIR FORCE INSTITUTE OF TECHNOLOGY

AIR UNIVERSITY
UNITED STATES AIR FORCE

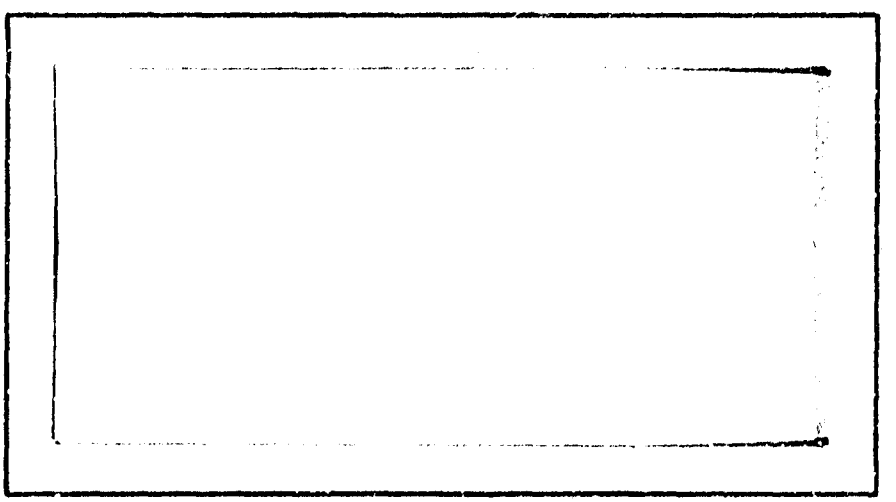

SCHOOL OF ENGINEERING

WRIGHT-PATTERSON AIR FORCE BASE, OHIO

UNCLASSIFIED
Security Classification

DOCUMENT CONTROL DATA - R & D

(Security classification of title, body of abstract and indexing annotation must be entered when the overall report is classified)

1. ORIGINATING ACTIVITY (Corporate author)
Air Force Institute of Technology (AFIT/EN)
Wright-Patterson AFB, Ohio 45433

2a. REPORT SECURITY CLASSIFICATION
UNCLASSIFIED

2b. GROUP

3. REPORT TITLE
Measurement of the Visible Reflectance Spectra of Orbiting Satellites

4. DESCRIPTIVE NOTES (Type of report and inclusive dates)
AFIT Thesis

5. AUTHOR(S) (First name, middle initial, last name)
Lambert, John V., Capt., USAF

6. REPORT DATE	7a. TOTAL NO. OF PAGES	7b. NO. OF REFS
March 1971	63	22

8a. CONTRACT OR GRANT NO.	9a. ORIGINATOR'S REPORT NUMBER(S)
N/A	AFIT Thesis GEP/PH/71-11
b. PROJECT NO. N/A	
c.	9b. OTHER REPORT NO(S) (Any other numbers that may be assigned this report)
d.	N/A

10. DISTRIBUTION STATEMENT This document is subject to special export controls and each transmittal to foreign governments or foreign nationals may be made only with prior approval of the Dean of Engineering, Air Force Institute of Technology (AFIT/EN), Wright-Patterson AFB, Ohio 45433.

11. SUPPLEMENTARY NOTES

12. SPONSORING MILITARY ACTIVITY
Aerospace Research Laboratories
General Physics Laboratory
Wright-Patterson AFB, Ohio 45433

13. ABSTRACT

Low resolution reflectance spectra of three orbiting satellites, objects 2253, 3819, and 4392, were measured using a scanning spectrometer designed and built for use with the Aerospace Research Laboratories satellite tracking telescope. The spectrometer, having a variable bandpass interference filter as the dispersive element, operates between 4000 and 7000 A with a resolution of 150 A. The required data reduction procedures were developed and the system was tested on astronomical objects. The measured reflectance spectrum of object 2253 is in agreement with that of the known surface material, aluminum. The measured reflectance spectra of objects 3819 and 4392 resemble those of white paints.

DD FORM 1 NOV 68 1473

UNCLASSIFIED
Security Classification

14. KEY WORDS	LINK A		LINK B		LINK C	
	ROLE	WT	ROLE	WT	ROLE	WT
Spectrometer						
Scanning Spectrometer						
Reflectance Spectrum						
Spectral Reflectivity						
Reflectance						
Reflectivity						
Satellite						
Artifical Satellite						

MEASUREMENT OF

THE VISIBLE REFLECTANCE SPECTRA

OF ORBITING SATELLITES

THESIS

GEP/PH/71-11 John V. Lambert
Captain USAF

MEASUREMENT OF
THE VISIBLE REFLECTANCE SPECTRA
OF ORBITING SATELLITES

THESIS

Presented to the Faculty of the School of Engineering of
the Air Force Institute of Technology
Air University
in Partial Fulfillment of the
Requirements for the Degree of
Master of Science

by

John V. Lambert, B.S.
Captain USAF

Graduate Engineering Physics

March 1971

Preface

My interest in optical observations of orbiting spacecraft began during my assignment to the Air Force Avionics Laboratory. I had been especially interested in the work being done by Dr. K.E. Kissell and others at the Aerospace Research Laboratories Sulphur Grove Facility, so I was delighted with the opportunity to do my thesis work there. The proposed topic, measurement of the spectral reflectivity of satellites, was very appealing since no previous work had been done in this area.

I would like to thank Dr. L.S. Pedrotti, my AFIT thesis advisor, for allowing me to take this project, and Dr. K.E. Kissell, my laboratory supervisor, for his timely direction and counsel. I would also like to thank the many ARL personnel who assisted me during this period, especially Mr. R.C. Vanderburgh and Captain L.S. Nicknik.

Contents

List of Figures

List of Tables

Abstract

Low resolution reflectance spectra of three orbiting satellites, objects 2253, 3819, and 4392, were measured using a scanning spectrometer designed and built for use with the Aerospace Research Laboratories satellite tracking telescope. The spectrometer, having a variable bandpass interference filter as the dispersive element, operates between 4000 and 7000 Å with a resolution of 150 Å. The required data reduction procedures were developed and the system was tested on astronomical objects. The measured reflectance spectrum of object 2253 is in agreement with that of the known surface material, aluminum. The measured reflectance spectra of objects 3819 and 4392 resemble those of white paints.

GEP/PH/71-11

MEASUREMENT OF THE VISIBLE REFLECTANCE SPECTRA OF ORBITING SATELLITES

I. Introduction

Background

Optical observations of artificial satellites began shortly after the launching of the first Soviet Sputnik in 1957; these observations were primarily concerned with determining the satellite orbits. Few attempts were made before 1964 to analyze the reflected light to determine a satellite's physical or dynamic characteristics. Since that time techniques have been developed, primarily at the Air Force Aerospace Research Laboratories, for the measurement of the brightness of orbiting spacecraft with accuracies sufficient for detailed analysis. To date, these analyses have included determination of satellite shape, dynamics, and surface scattering properties, dielectric constant, and color indices.

Analysis of the reflectance spectrum of a satellite using the techniques of reflectance spectroscopy can permit identification of the satellite surface materials and monitoring of changes in the materials due to the space environment. In classical astronomy, these techniques have been successfully applied to the determination of the surface composition of the moon and asteriods.[1,2] Previous spectral measurements on satellites have been

limited to either visual estimates of color[3] or broadband measurements using the standard astronomical UBV filters.[4,5] These observations provide information on the gross spectral reflectance, but do not permit detailed analysis. The object of this study is to demonstrate the feasibility of measuring low-resolution visible reflectance spectra of orbiting satellites.

Scope of Study

This report will detail the development of both equipment and procedures for the measurement of the reflectance spectra of orbiting spacecraft to be used in conjunction with the existing ARL satellite tracking facilities at Sulphur Grove, Ohio. The techniques developed differ from those used in spectral studies of astronomical objects. Special consideration had to be given to compensating for the large changes in the brightness of a satellite due to its dynamic motions about its center of mass. These variations in brightness can typically amount to two orders of magnitude within a few seconds. In common with the astronomical problems, however, are the difficulties encountered in spectral studies of low-intensity sources since artificial satellites are seldom brighter than the average stars or planets.

The problem was resolved into three major divisions: the development of a technique for determining the spectral reflectance of a satellite; the design, construction, and testing of a suitable spectrometer; and the establishment

of data handling and reduction procedures. Unless otherwise noted, the work presented in this thesis is orginal and that of the author.

II. Theory

Optical Observations of Spacecraft

Satellite Visibility. The visibility of an orbiting satellite to an observer on the ground is a function both of the brightness of the satellite and the contrast between the satellite and the sky. The contrast, C, is defined as:

$$C = \frac{B_s - B_b}{B_s + B_b} \qquad (1)$$

where B_s is the brightness of the satellite and B_b is the brightness of the sky. The brightness of the satellite depends on its size, shape, surface properties and orientation, as well as the illumination and range. The apparent brightness of the sky is the result of atmospherically scattered light from the sun, moon, stars, and terrestrial sources, and atmospheric emission, "airglow".

To maximize the contrast between the satellite and the sky, hence, to increase the visibility of the satellite, most optical observations are made during the twilight hours before sunrise and after sunset. At these times, the sun is below the observer's horizon so the sky brightness is reduced to near minimal levels. However, the satellite, at some distance above the surface of the earth, can still be illuminated by the sun (Fig. 1). For passive observations, the sun is assumed to be the only source of illumination. Other sources, such as stars or reflected light from the earth or moon, are of such low intensities as to be negligible in

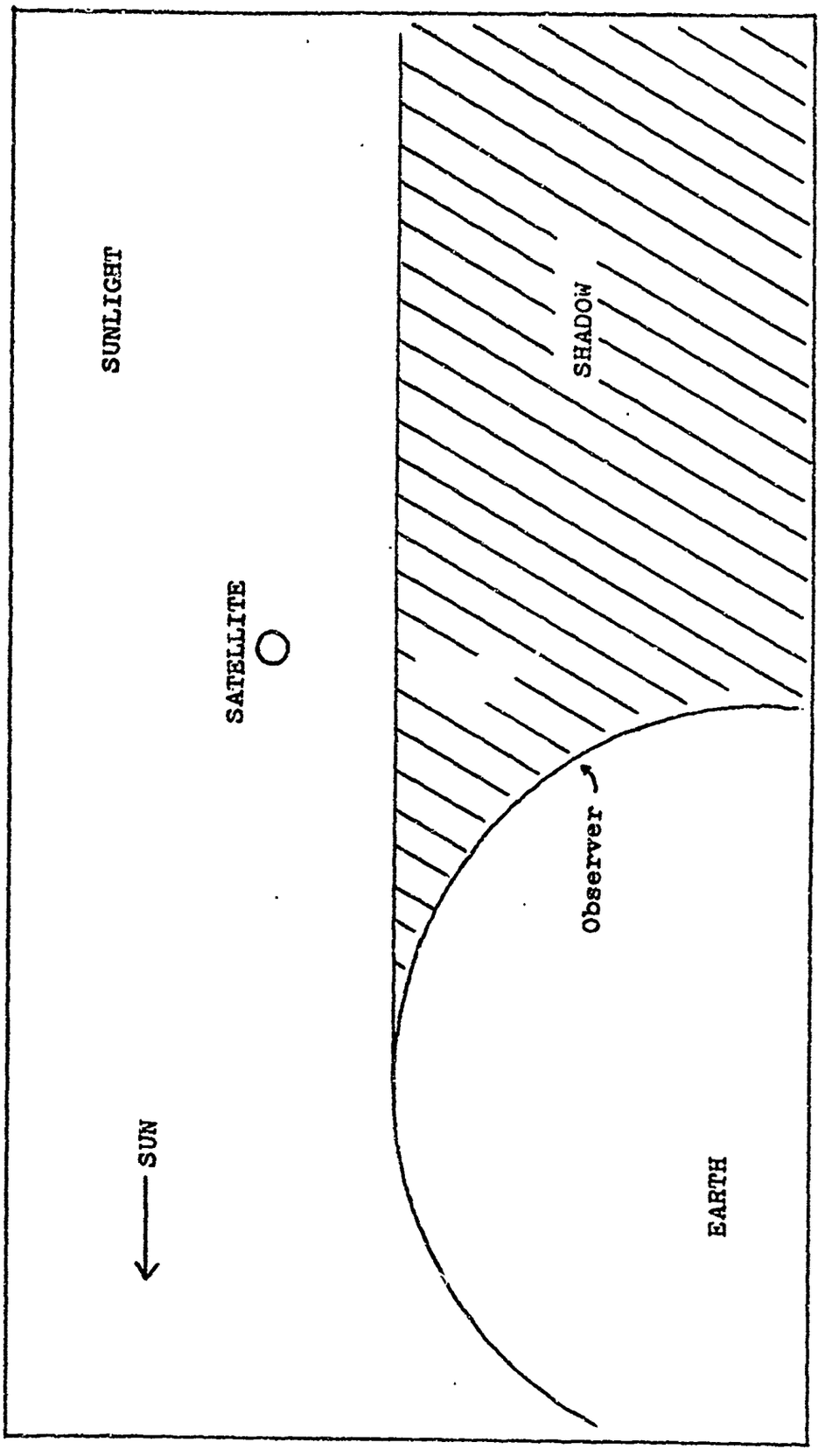

Fig. 1. Satellite visibility criteria.

comparision to the intensity of the solar radiation.

Satellite Brightness. The observed brightness of many satellites can be predicted by assuming the satellite is composed of a combination of simple geometric surfaces: planes, spheres, cylinders, or cones. The angular dependence of the reflectance is computed separately for each surface, and the results combined to yield the observed brightness of the satellite as a function of the relative positions of the sun and the observer, and the orientation of the satellite. In general, the brightness will vary depending on the "phase angle", the angle between the sun and the observer as measured from the satellite, and the orientation of the satellite body axis relative to these directions. Expressions describing the reflectance for simple surfaces have been derived by the author[6] and others; Kissell[4] presents a comprehensive bibliography for the derivations.

The observations at the ARL Sulphur Grove Facility are directed principally toward the measurement of the apparent satellite brightness. The records of the observed brightness as a function of time, commonly referred to as "light curves", are analyzed to determine a satellite's physical and dynamic properties. The analyses are based on comparisons to the theoretical models.

Stellar Magnitude System. The observed brightness of a satellite is normally expressed in units of stellar magnitude. This magnitude system is used in classical astronomy to describe the brightness of the stars. In the system, one

unit of magnitude corresponds to a ratio of the brightnesses of two sources of 2.512. This value was chosen for compatibility with an earlier system in which the visible stars were divided into six groups according to their apparent visual brightness. The magnitude difference between two sources is related to their brightnesses by:

$$-(m - m_*) = \log_{2.512}(F/F_*) \qquad (2)$$

where m and m_* are the respective magnitudes of the two sources, and F and F_* are the observed fluxes. The magnitude of a star or satellite can be found by comparing the observed flux to that of a zero magnitude source. For visual observations, a zero magnitude source is defined to have an exo-atmospheric flux equivalent to 2.43×10^{-4} lumens/meter^2. Similar magnitude standards have been defined for other types of measurements.

Measurement of Reflectance Spectra

In general, the surface of a satellite will selectively reflect or absorb certain wavelengths giving rise to a reflectance spectrum that is uniquely characteristic of the chemical composition of the surface. The following section will be concerned with developing a technique for the measurement of this spectrum. The interested reader is referred to Kortum[7] for a detailed theoretical treatment of reflectance.

Definition. The absolute spectral reflectivity of a surface is defined as the ratio of the reflected flux to the incident flux at each wavelength:

$$R_\lambda = F_\lambda^r / F_\lambda^i \qquad (3)$$

where R_λ is the reflectivity of the surface at wavelength λ and F_λ^r and F_λ^i are the reflected and incident monochromatic fluxes, respectively. The reflectivity is a function of the angle of incidence of the illuminating flux, but, only in the case of grazing incidence does this angular dependence affect the relative characteristics of the reflectance spectrum. Experimental measurement of the absolute reflectance requires measurement of both the total incident and the total reflected flux. In the case of satellite observations, neither of these quantities can be determined unless a priori information is available as to the satellite size, shape, orientation, and surface scattering properties.

Measurement of the relative spectral reflectivity is possible, however, by comparison of the spectral distribution of the observed reflected light to that of the incident light. Differences in the relative spectral distributions can be attributed to selective absorption and reflection by the satellite surface. This relative spectral reflectivity, r_λ, may be defined as:

$$r_\lambda = F_\lambda^o / F_\lambda^i \qquad (4)$$

where F_λ^o and F_λ^i are the observed and incident monochromatic fluxes, respectively. The relative spectral reflectivity will be proportional to the absolute spectral reflectivity except in the case of large incidence and observation angles where the direction distribution of the reflected flux can

become wavelength dependent. For satellite observations, these large phase angles would be attained only if the sun, satellite, and observer were nearly aligned, a condition which violates the visibility criteria.

Atmospheric and Instrumental Effects. The observed spectral distribution of the light reflected from a satellite is altered by atmospheric transmission and instrumental sensitivity. The atmospheric effects, arising from Rayleigh scattering and selective absorption, are a function of the intervening air mass. The exact magnitude of the effects is, however, highly variable, both temporally and spatially. The instrumental effects result from the spectral characteristics of the optics and the quantum efficiency of the detector. For an absolute comparison of the spectrum of the light reflected from a satellite to the illuminating solar spectrum, the atmospheric and instrumental effects must be accurately determined and eliminated.

These effects may also be eliminated by a direct comparison of the observed spectrum to a solar spectrum obtained under identical conditions, i.e., with the same instrument and through an equivalent atmospheric path. In this way, both spectra are subject to the same distortions which will be removed when the ratio of the fluxes at each wavelength is taken in the calculation of the relative spectral reflectivity. This direct comparison technique is practical under experimental conditions because of the presence of many sunlike stars throughout the sky. The

required solar reference spectrum can be obtained by measuring the spectral distribution of the light from one of these stars. To satisfy the requirement for an equivalent atmospheric path, the star must be at the same elevation at which the satellite was observed, and the measurement must be made close to the time of the satellite observation.

Reference Stars. The choice of the reference stars will be based on standardized multicolor photometric measurements available in the literature. The spectral distribution of the light from many stars has been measured using standard wide-band filters with passbands of 500 to 800 Å. The measurments, expressed in stellar magnitudes, provide a comparison of the emission of the stars within prescribed wavelength intervals in the ultraviolet (U), blue (B), visible or green (V), red (R), and infrared (I) to the emission of a specific standard of both brightness and color. Since the measurements are expressed in stellar magnitudes, differences between the values represent ratios of the fluxes within these spectral regions. The differences, referred to as color indices, thus provide a measure of the relative spectral energy distributions of the stars, usually referenced to the visible or V band. The relative spectral distribution is independent of the apparent brightness of the star, and is indicative of the star's temperature or spectral type. The visible magnitude, related to the apparent brightness of the star, is normally reported with the color indices. This tabulation then allows an inter-

comparison of both the brightnesses on an absolute basis and the color indices on a relative basis.

A good approximation to the relative solar energy distribution can be obtained by choosing as reference stars those stars whose multicolor indices closely match those of the sun. Two principle lists of modern stellar multicolor indices have been recently published. The Arizona-Tonantzintla Catalogue[8] contains the five-color indices for all stars brighter than +5 stellar magnitude, and the Eggen list[9] contains three-color indices (UBV) for 1,066 of the nearer G-type stars. A selected list (Table I) has been prepared from these references of the G-type stars used in this study and representative stars of other spectral types.

Table I

Multicolor Indices for Selected Stars

		Magnitude					
Star	Type	V	U-V	B-V	V-R	V-I	Ref
15 Mon	07	4.66	-1.31	-0.24	-0.99	-0.31	8
β Cep	B2 III	3.23	-1.17	-0.21	-0.10	-0.32	8
α Lyr	A0 V	0.00	0.03	0.00	-0.04	-0.07	8
α Lep	F0 Ib	2.58	0.47	0.19	0.22	0.43	8
14411	dGo	5.50	0.88	0.68	--	--	9
Sun	dGo	-26.72	0.70	0.64	0.52	0.78	4
24 Cas	G0 V	3.43	0.62	0.58	0.50	0.86	8
iota Per	G0 V	4.07	0.77	0.59	0.54	0.83	8
λ Aur	G0 V	4.70	0.75	0.60	0.52	0.83	8
30 Cas	G0 Vp	5.12	0.78	0.69	--	--	9
α Cas	K0 II-III	2.22	2.30	1.17	0.79	1.38	8
δ Lyr	M4 II	4.30	3.32	1.67	1.79	3.42	8

III. Equipment

ARL Sulphur Grove Facility

The Aerospace Research Laboratories Sulphur Grove Facility has been described in detail in previous publications.[4,10,11] Only a brief description of the facility will be given here with emphasis placed on those items affecting the present study.

Physical Plant. The facility is located at Sulphur Grove, Ohio, four and one-half miles northeast of Dayton, Ohio. There are three buildings on the site--the tracking building, the equipment building, and a trailer. The tracking building houses the telescope and the electronics associated with the mount drives. The photometer electronics and the timing and recording equipment are in the equipment building. Electrical connections between the tracking and equipment buildings are made through a covered trough. A darkroom and a teletype terminal over which satellite position predictions are received are also located in the equipment building. The trailer contains work areas and an optics laboratory.

Telescope. The telescope is a 61-cm, f/16, Cassegrain reflector (Fig. 2). A beam-splitter cell just before the focus allows the image to be formed at either or both of two locations. One location contains a framing camera used in direct photography of orbiting spacecraft. The other location contains the photometer. In normal operations, all the light is directed to the photometer. An Astro-Mechanics,

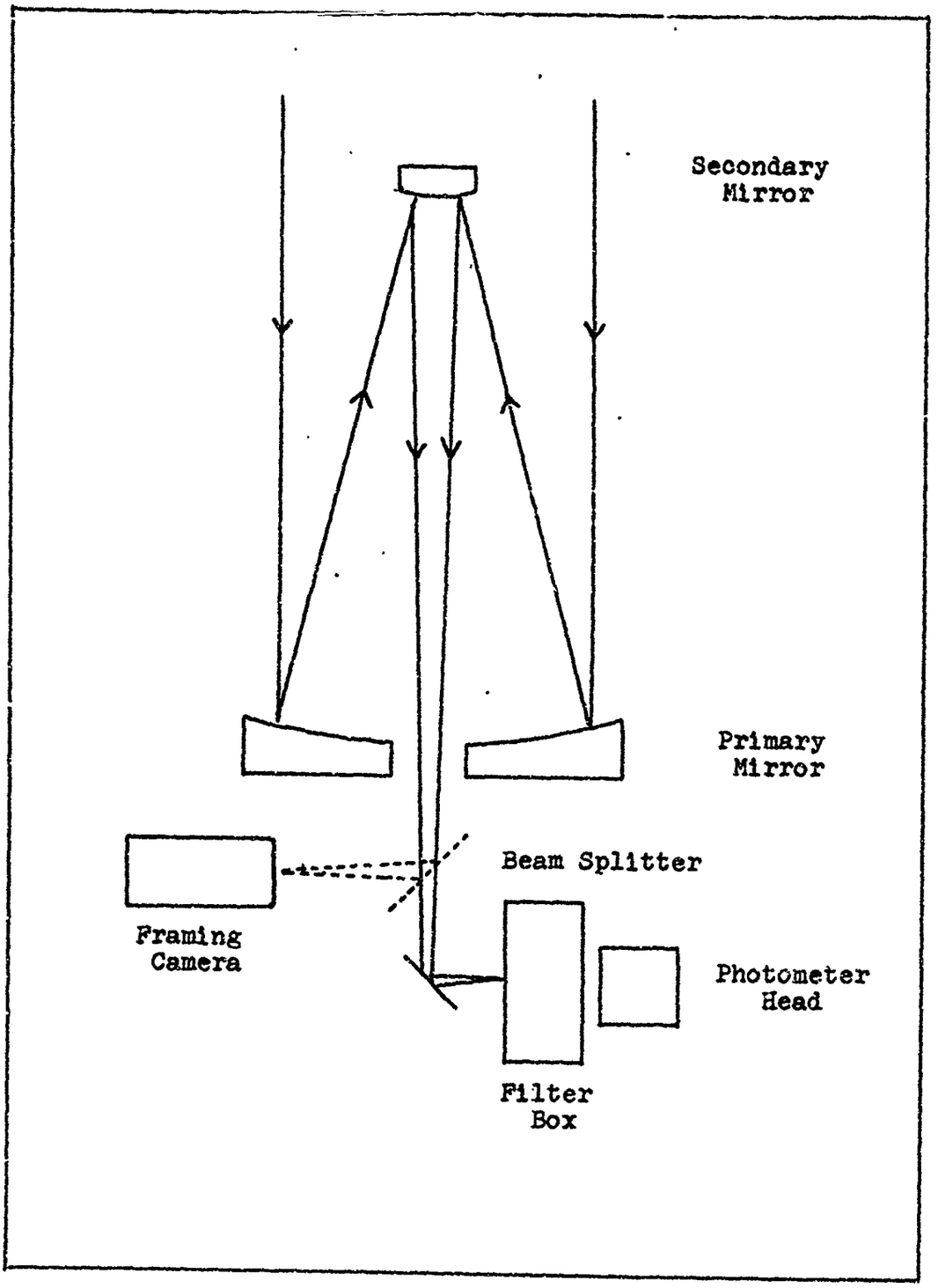

Fig. 2. Schematic of ARL Telescope and Associated Optics.

Inc. filter box containing aperture masks, filter, and re-imaging optics preceeds the photometer. The aperture masks are used to restrict the area of the sky imaged onto the photocathode. The use of smaller apertures thus lowers the sky-brightness signal; however, as the aperture size decreases, the tracking accuracy requirements become more stringent. A circular aperture equivalent to 110 arc-seconds in diameter when projected against the sky was used throughout this study. Other apertures available are 57, 24, 14, and 9.5 arc-seconds. The aperture masks are mounted on an indexed disk in the focal plane of the telescope. Also in the filter box is an indexed wheel for mounting 25-mm square optical filters. Normally included are the standard astronomical UBV filters. A quartz Fabry lens is used to image the 61-cm primary onto the photocathode of the detector. For checking telescope focus and alignment, the filter box contains a microscope assembly which can be introduced into the optical path with a movable mirror.

Acquisition and tracking of satellites is performed visually using one of two tracking telescopes aligned with the optical axis of the main instrument. The prime tracking telescope is a 12.5-cm aperture refractor with two turret-mounted eyepieces providing 1° and 6° fields-of-view, respectively. Acquisition is normally performed using the wide field-of-view, and tracking using the narrow field-of-view. For acquisition and tracking of faint targets, a 20-cm Schmidt-Cassegrain reflector is used.

The telescope mount is a special four-axis design developed by Kissell and Nunn.[12] The four axes allow the telescope to be oriented so that an artifical satellite can be tracked along one axis. The telescope describes a small circle on the celestial sphere, approximating the apparent satellite trajectory. Tracking along the one axis is performed by a rate command. Errors orthogonal to the small circle approximation are compensated by a motorized position control on a second axis.

Logarithmic Photometer. The performance of the photometer will be described in the following chapter. An RCA-4526, 11-stage photomultiplier tube is used as the detecting element. This tube has a modified S-20 response (Fig. 3) allowing detection from about 3000 to 8000 Å. The photometer signal is obtained by sampling the potential across the photomultiplier tube with a voltage divider. A bias potential is introduced to bring the signal within the range of the recording equipment.

Recording Equipment. The photometer signal is recorded on both a Honeywell Model 1508 Visicorder and an Ampex Model SP-300 tape recorder. The Visicorder provides an immediate visual record of the photometer signal, while the tape provides a permanent record for later playback. The tape can then be played back into the Visicorder and the record expanded or compressed as required for data extraction. Recorded simultaneously with the photometer signal is the National Bureau of Standards WWV timing broadcast.

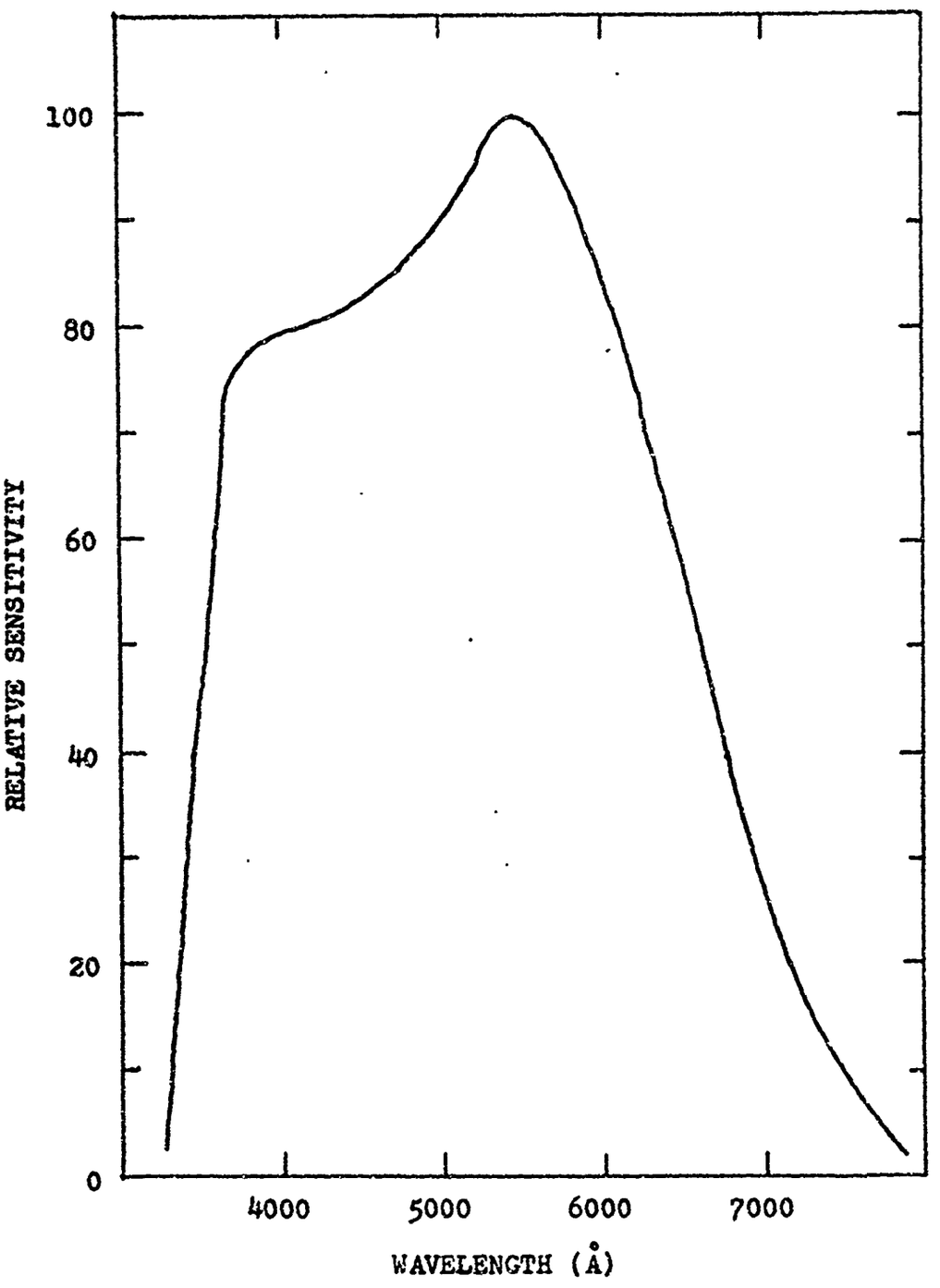

Fig. 3. Modified S-20 photocathode response.

Scanning Spectrometer

A single-channel, scanning spectrometer operating between 4000 and 7000 Å with a nominal resolution of 150 Å was designed and built for this study. The design considerations and the mechanical details of the instrument are discussed below.

Design Considerations. The design of the spectrometer is influenced by two basic constraints--the characteristics of the light reflected from a satellite, and the necessity of interfacing with the existing equipment. Because of the low intensity of the reflected light, the instrumental efficiency must be high. The apparent visual magnitude of an artifical satellite rarely exceeds +1 stellar magnitude, and the ARL system is capable of detecting targets down to +11 stellar magnitude. The spectrometer is designed to operate over as much of this range (10,000 to 1) as possible. Since the temporal variations in the intensity of the light reflected from a satellite could be misinterpreted as spectral features, the spectrometer design provides for rapid scanning of the spectral region to minimize these intensity variations during a scan. To account further for these variations broadband or undispersed measurements are also made during a scanning cycle to monitor the overall intensity and allow analytical corrections for periodic variations.

Although the ARL telescope is designed to accept up to 100 kg of equipment at the Cassegrain focus, certain

mount clearance restrictions dictated as compact an arrangement as possible for the spectrometer. This constraint, coupled with those of high optical efficiency and rapid scan rates, led to the selection of a variable-passband interference filter for the dispersive element rather than a prism or grating device. The spacer layer of one of these filters varies in thickness across the filter producing corresponding variations in the passband wavelength. A semi-circular filter having a linear variation of the passband with circumference was produced for this study by Optical Coating Laboratories, Inc. (OCLI). This filter is now a standard OCLI product although those tested here were the first ever fabricated in this form. The use of this filter has permitted a simple scanning mechanism and has resulted in an extremely compact arrangement for the spectrometer.

The design of the spectrometer seperated into two problems, the design of a monochromator and the selection of a suitable detector. Because of its wide dynamic range and rapid response, the AHL photometer was retained as the detector of the scanning spectrometer. The original photomultiplier tube having an S-17 response was replaced by the RCA-4526 tube because of the improved red response of the S-20 photocathode.

<u>OCLI Filter</u>. The design of the monochromator centered about the dispersive element, the variable-bandpass interference filter. Three of the OCLI filters were obtained (Fig. 4). The transmission of each filter was measured

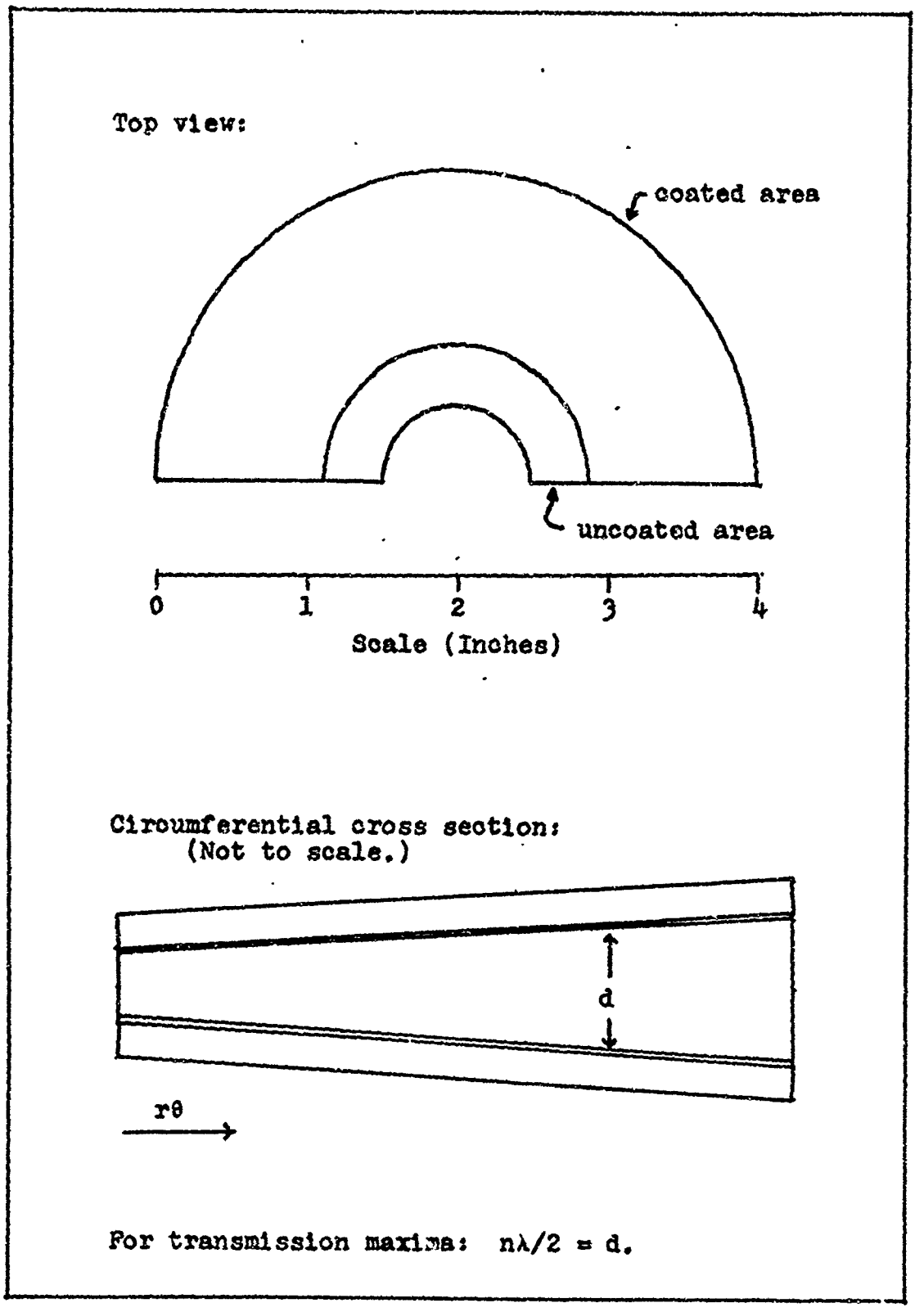

Fig. 4. OCLI variable bandpass interference filter.

from 3000 to 8000 Å (the region covered by the photomultiplier tube response) at 10^{o} increments about the circumference using a Cary Model 14R Spectrophotometer. The filter which combined the highest transmission with the narrowest passband was selected for use in the spectrometer.

The transmission of this filter as a function of wavelength for three angular positions is shown in Figure 5. The results of the measurements are summarized in Table II. An equation relating the wavelength of the passband peak to the angular filter position was obtained by fitting a straight line to the first-order transmission data of Table II using a least-square procedure. The resulting equation is:

$$\lambda = 3790 \text{ A} + 19.7 \text{ Å/degree} \times \theta \qquad (5)$$

where λ is the wavelength of the passband peak in Angstrom units, and θ is the angular filter position in degrees measured from the "blue end" of the filter. The rms error in fitting the line to the data points was 36 Å; as will be seen, this error is small compared to other uncertainties affecting the measurements.

In order to use the filter to obtain accurate intensity measurements at a given wavelength, it is necessary to eliminate the higher-order passbands, restricting transmission to the first order. Since the shortest-wavelength first-order transmission occurs at 4020 Å and the longest-wavelength second-order transmission occurs at 3770 Å, the

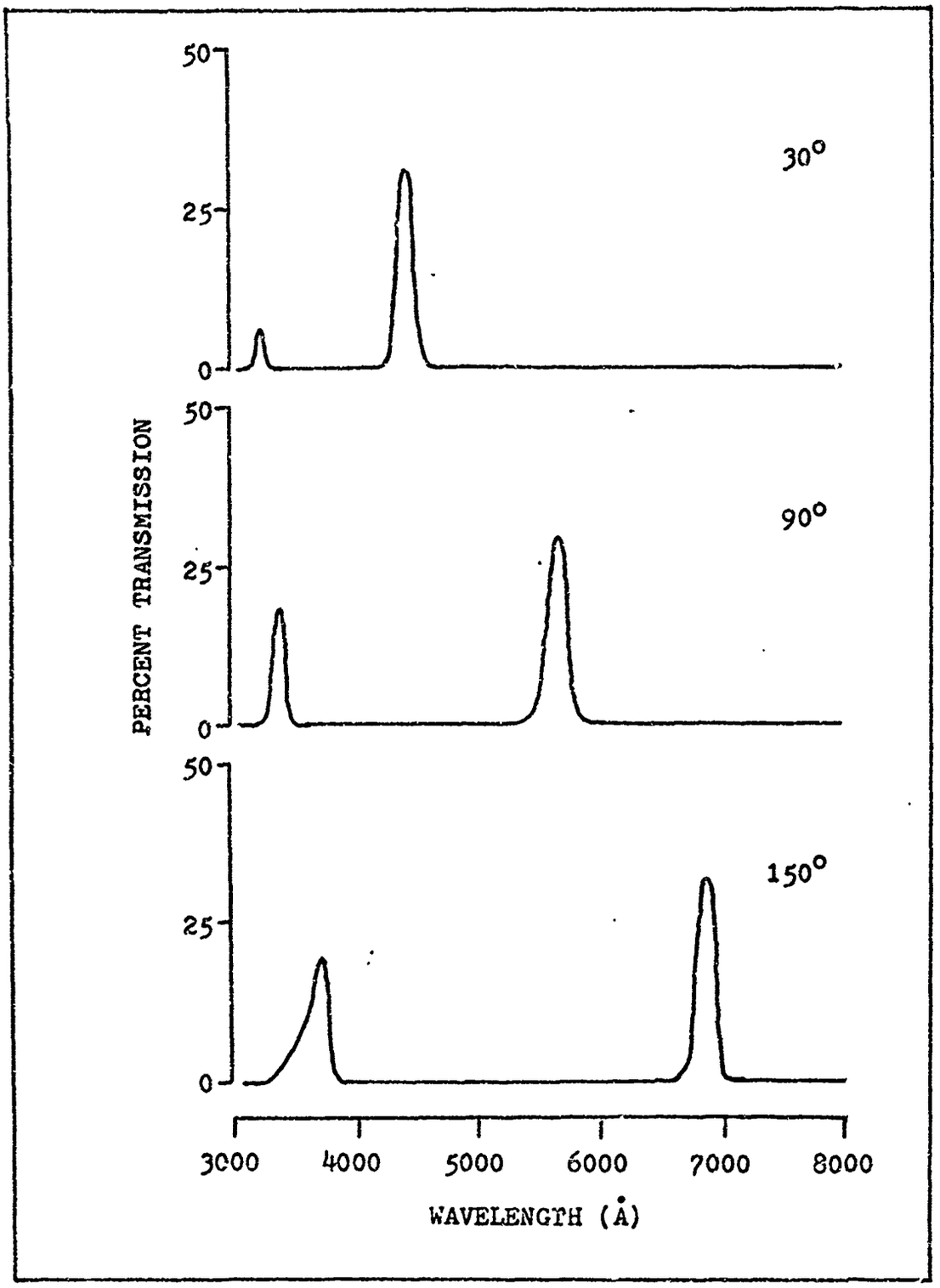

Fig. 5. Transmission of OCLI Filter. (For indicated angular positions.)

Table II
OCLI Filter Transmission Measurements

Filter Position (degrees)	First Order			Second Order		Third Order
	Maxima (Å)	% Transmission	FWHM* (Å)	Maxima (Å)	% Transmission	Maxima (Å)
10	4020	28	160	--	--	--
20	4220	30	150	--	--	--
30	4390	31	150	3210	4	--
40	4520	30	140	3210	3	--
50	4770	29	130	3230	4	--
60	4980	29	130	3240	6	--
70	5170	29	130	3230	5	--
80	5370	30	130	3240	12	--
90	5590	28	140	3280	17	--
100	5780	29	140	3300	23	--
110	5910	29	130	3320	25	--
120	6130	29	140	3340	29	--
130	6260	30	140	3400	27	--
140	6550	30	150	3450	21	--
150	6780	30	150	3620	23	3210
160	6990	32	150	3700	29	3210
170	7180	31	160	3770	32	3210

*Full width of filter passband at half maximum.

ideal solution would be a filter with zero transmission below 3900 Å and one-hundred percent transmission above 3900 Å. A Jenaer Glaswerk Schott & Gen., type GG-22 filter was chosen as the closest commerical filter to this ideal from those examined. The transmission spectrum of one of these filters was measured using the Cary Model 14R Spectrophotometer (Fig. 6). By using the GG-22 filter in conjunction with the OCLI variable-bandpass interference filter, accurate measurements can be made from 4000 to 7000 Å. At 7000 Å, the second-order passband reaches a maximum transmission of eight percent as compared to the thirty-two percent transmission for the first order. For the solar spectral distribution, the flux transmitted by the second order passband will be eighteen percent of the first order transmission.

Since the passband location and band-width of an interference filter are dependent on the convergence angle of the beam in which it is used, some consideration was given to the necessity for collimating optics in the spectrometer. The converging beam of the f/16 telescope corresponds to a convergence angle of 3.6° so the maximum effect could be estimated. Calculations and experimental measurements by Lissberger and Wilcock[13] indicate that for a filter with a 150 Å passband negligible degradation in the filter performance would occur in this beam. Thus, the OCLI filter can be used directly in the telescope optical path with no collimating optics.

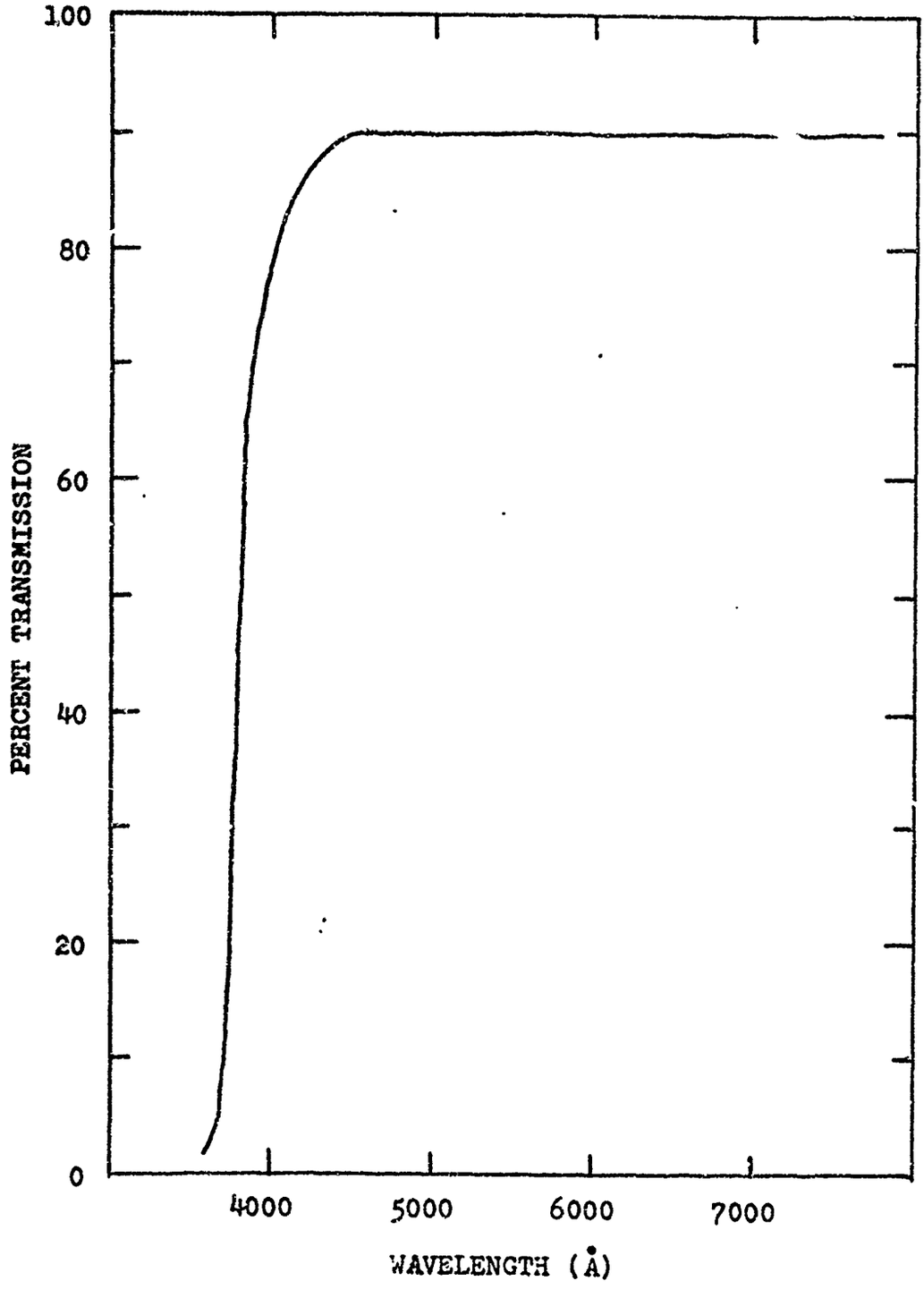

Fig. 6. Transmission of Schott GG-22 Filter.

The passband width is also affected by the circumferal extent of the area of the filter through which light is transmitted. In order to minimize the transmitting area the filter must be used near the focal plane of the telescope where this area corresponds to the image size itself. The image of an orbiting satellite is normally less than one millimeter in diameter with the ARL telescope. Near the outer circumference of the OCLI filter this image will have a negligible effect on the filter passband. However, the satellite image may be located anywhere within the 110 arc-second field aperture. This uncertainty in the location of the image produces an uncertainty in the wavelength at which measurements are being made. The uncertainty associated with the 110 arc-second aperture is on the order of 60 Å, which is comparable to the filter passband.

Mechanical Components. The mechanical components of the spectrometer were constructed by the ARL shops. Construction involved three items--1) fabrication of a filter cell, 2) modification of the Astro-Mechanics, Inc. filter box, and 3) fabrication of a spacer to permit the assembly to be mounted on the telescope.

The basic function of the filter cell is to hold the OCLI filter securely in place and to allow it to be rotated past the entrance aperture of the filter box. A sketch of the filter cell is shown in Figure 7. The design of the cell is such that two filters might be used to obtain two

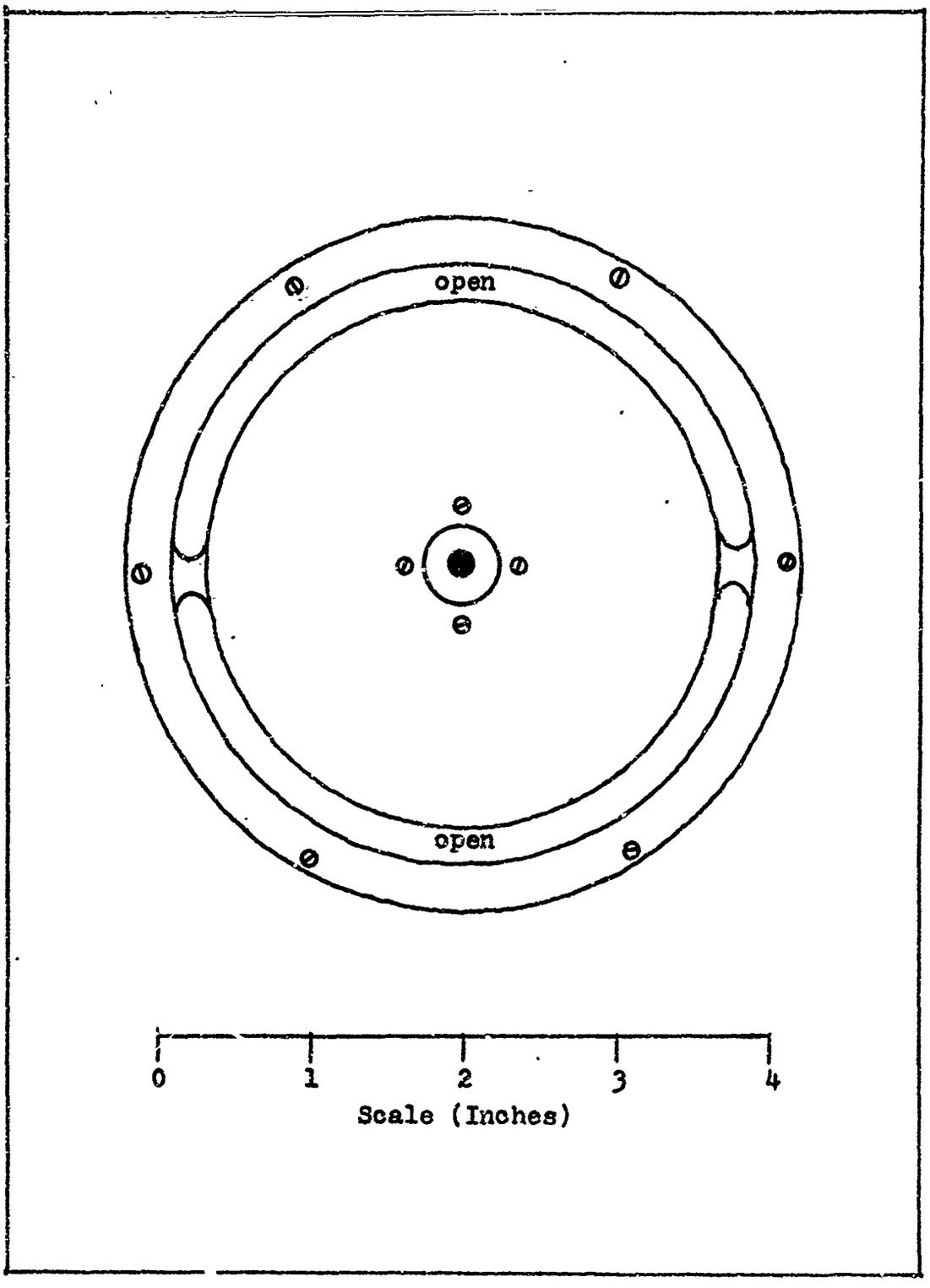

Fig. 7. Filter Cell.

wavelength scans per rotation cycle, or only one semi-circular filter used and a dispersed scan and a broadband measurement obtained per cycle. In the one-filter configuration, a counterweight is used in place of the second filter. In order to monitor the overall temporal variations in the light reflected from a satellite, the one-filter configuration was used in this study. The filter cell mounts directly on the shaft of the scanning motor.

The Astro-Mechanics, Inc. filter box forms the basic structure of the spectrometer (Fig. 8). The scanning motor, a Hurst Type PC DA, 30-rpm, synchronous motor, was mounted inside the filter box with the shaft extending through the base plate containing the aperture disk. The position of the motor was chosen so that the open area of the filter cell would be centered over the aperture during scanning. To accept the motor in this position, minor modifications to the filter box focusing-mirror assembly were required. Figure 9a shows the filter box with the filter cell mounted on the scanning motor shaft. The spacer was required to provide sufficient clearance between the filter box and the telescope mounting plate to allow rotation of the filter cell, and form a light-tight seal.

Operation. The assembled spectrometer, including the photometer is shown in Figure 9b. A foil shutter, covering the 60° segment immediately before the OCLI filter, was added to the filter cell to allow for the photomultiplier transient in going from the relatively bright open obser-

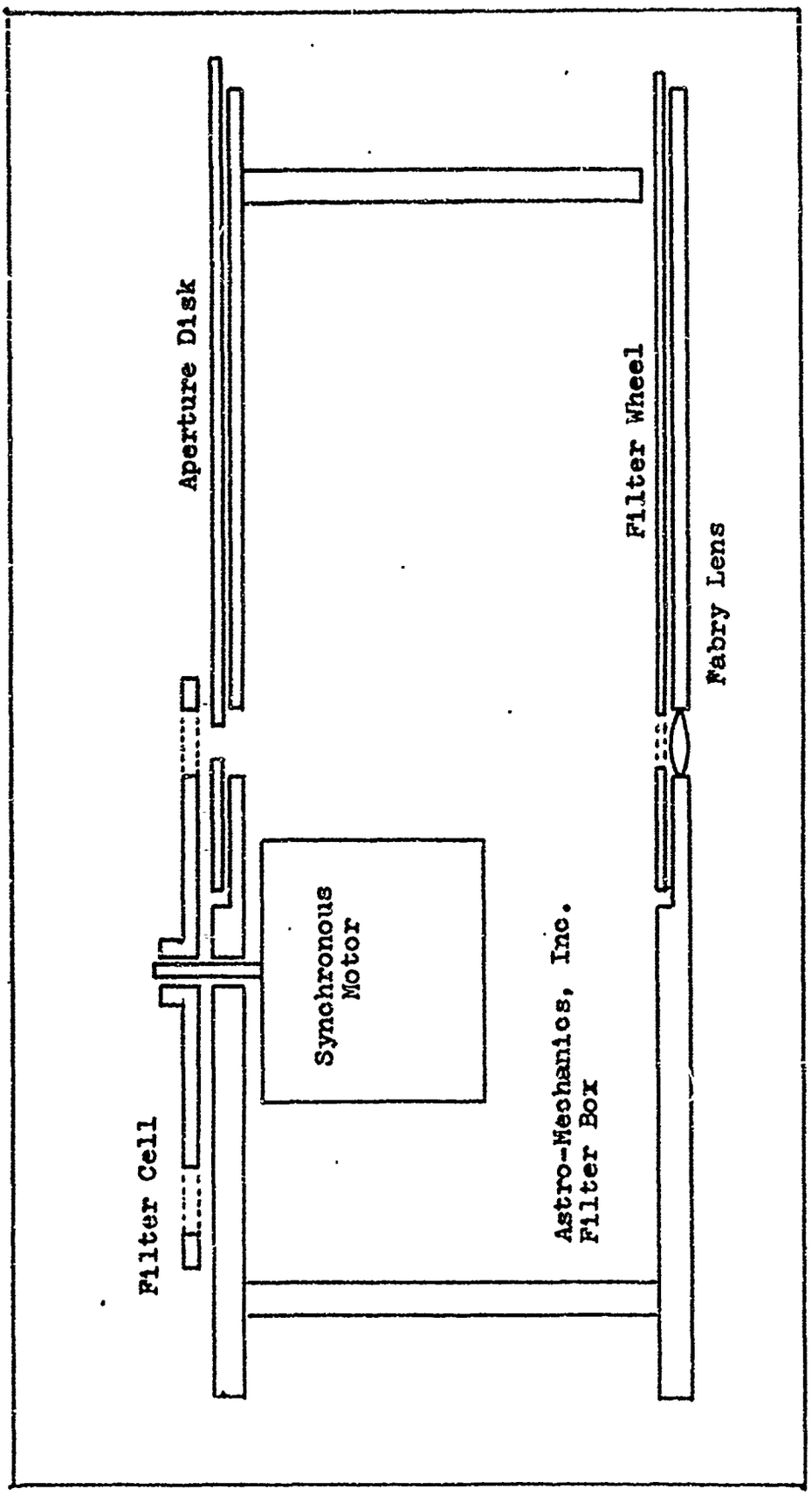

Fig. 8. Modified Filter Box.

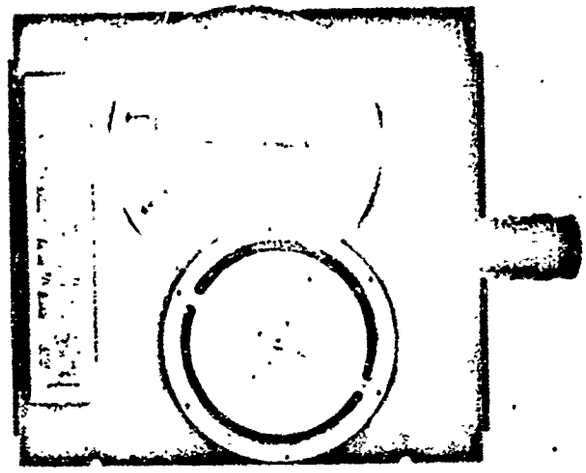

Fig. 9a. Top view of spectrometer showing filter box, aperture disk, and filter cell.

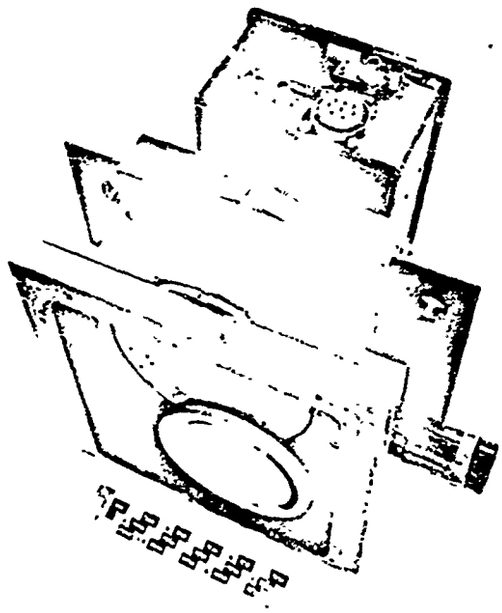

Fig. 9b. General view of spectrometer showing photometer head.

vation to the observation through the filter. This shutter also provides a sampling of the dark current signal during each scanning cycle. The spectrometer scans continuously in two-second cycles. Each cycle contains a broadband measurement, a dark current measurement, and a spectral scan from red to blue (Fig. 10).

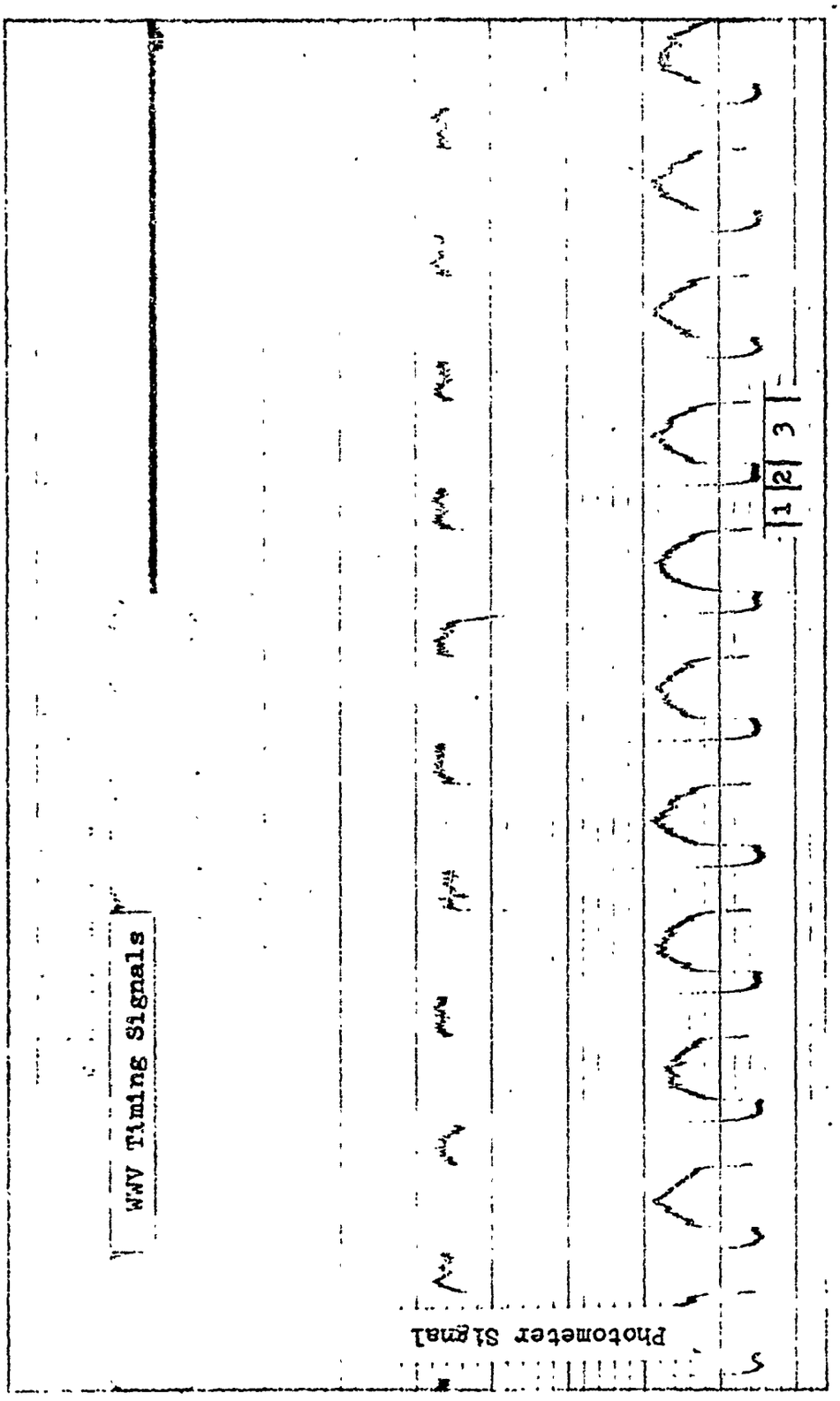

Fig. 10. Spectrometer Scanning Cycle. (Key: 1-open, 2-shutter, 3-spectral scan)

IV. Experimental Procedures

The experimental procedures will be discussed in two sections, data collection and data reduction. The data collection procedures are basically those normally employed at the Sulphur Grove site for the broadband observation of satellites. The data reduction procedures, however, represent the first use of a digital computer in the reduction of the photometric light curves. Previously, data reduction at the site has been done using graphical techniques.

Data Collection

Look-Angle Predictions. Predictions for the ARL facility are prepared as look angles for the site by the NORAD Space Defense Center and then transmitted by teletype to the site. The predictions are prepared only for the transits of selected satellites meeting specific visibility criteria. Each prediction consists of the time, elevation, azimuth, and range, for seven points during the transit. To convert to the circle settings for the four-axis mount, an analog technique developed by Vanderburgh[14] is used. The predicted azimuth and elevation points for the transit are plotted on a meridional net, and the best small circle is then fitted to these points. The choice of this small circle approximation to the apparent satellite trajectory determines the four shaft angle settings: azimuth, elevation, declination, and track angle. Of these settings, only the track angle is a function of time.

Acquisition and Tracking. Just before the start of a transit, the telescope mount is set to the calculated angles with the track axis at the initial acquisition position. When the target is acquired in the wide field-of-view of the tracking telescope, tracking is initiated. The target is centered in the field using the track-axis rate control and the cross-track position control on the elevation axis. The eyepiece turret is rotated to provide the higher magnification and the target image is then guided into the aperture of the photometer. An audio tone varying in pitch with the brightness of the target is used to verify the presence of the image within the aperture. The spectrometer scanning motor is then started. Tracking is continued using the track-axis rate control and introducing cross-track position corrections as necessary until the track-axis limits are reached or the satellite goes into shadow.

Calibration. Two types of signal amplitude calibration are used. Before and after each set of measurements, a voltage calibration is obtained by sequentially applying sixteen standard voltages to the inputs of the tape recorder and Visicorder. These voltages permit conversion of the records from Visicorder galvanometer deflection to the photometer signal voltage. A calibration of the photometer system is obtained for the measurement session by observing a number of G-type stars of known brightnesses. These measurements also provide data for a measurement of the atmospheric extinction. The time of each observation is

recorded for later calculation of the elevation of the star. The National Bureau of Standards WWV broadcast is recorded simultaneously with the photometer signal for accurate time calibration of the records. The only changes in the standard calibration procedures incorporated in this study were the spectral measurements of the stars and the inclusion of a number of stars at or near the observed elevations of the satellite.

Data Reduction

Previous comparative photometric studies using the ARL system have made use of empirical relations between target brightness and the photometer signal. A calibration curve was generated using measurements of G-type stars of known brightness and intermediate points obtained either by graphical interpolation or by use of an empirical curve fitted to the data.[4] The following discussion describes the derivation of an analytic expression relating the flux incident on the photocathode to the photometer signal and the application of the results to the measurements of the spectral reflectivity.

System Equation. The photometer in use at the ARL Sulphur Grove site is based on a design by M.H. Sweet.[15] This design employs a logarithmic range compression to permit operation over a range of target brightnesses on the order of 10^6:1. A simplified schematic of the photometer electronics is shown in Figure 11. The circuit

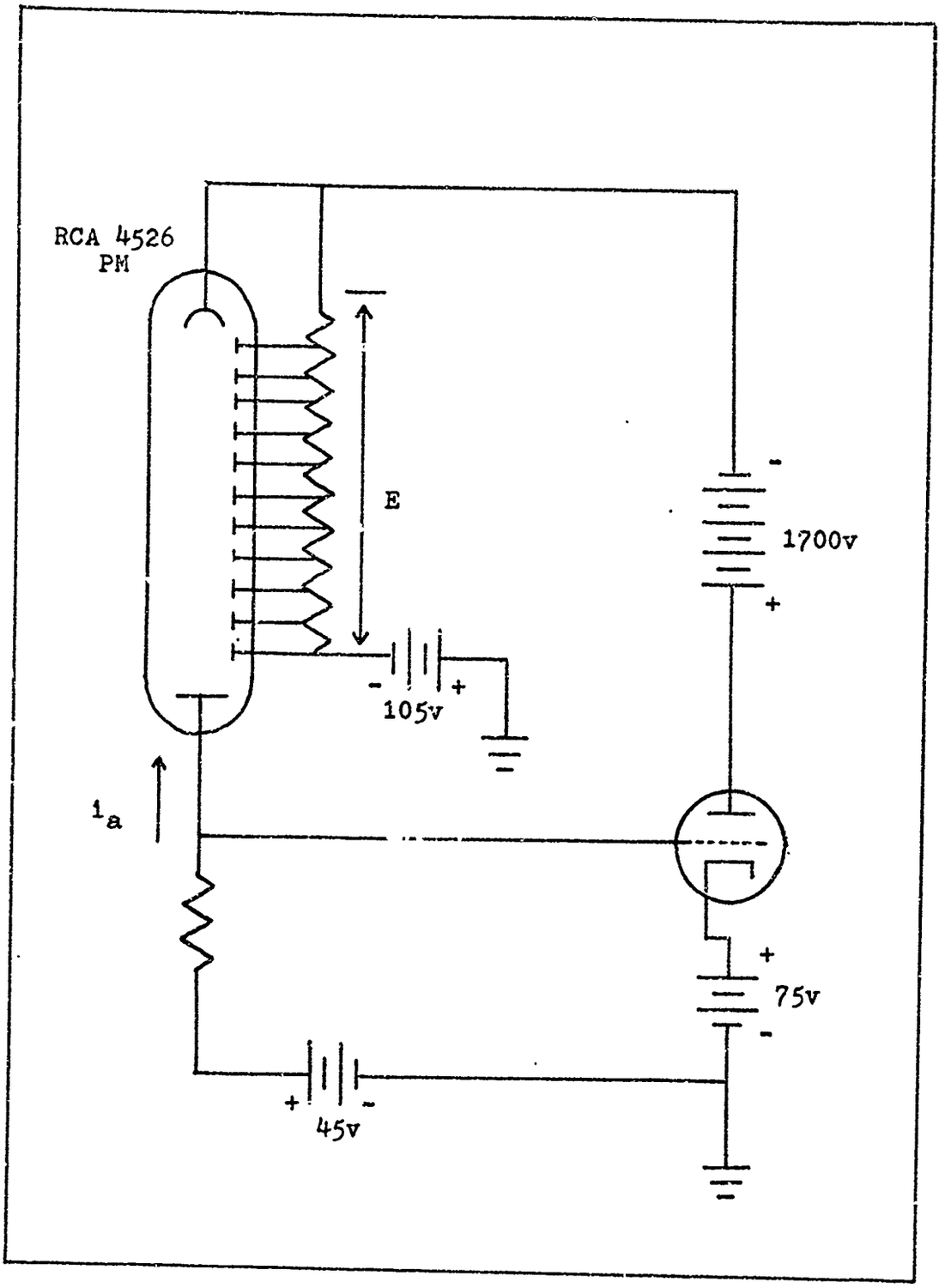

Fig. 11. Schematic of ARL Photometer Electronics.[16]

holds the anode current, i_a, constant by varying the photomultiplier tube dynode voltage, E_d. The relation between the flux incident on the photocathode, F, the anode current, and the dynode voltage is:

$$i_a = m F E_d^{n\beta} \tag{6}$$

where m is a system constant which includes the luminous sensitivity of the photocathode, n is the number of dynode stages, and β is the relative dynode secondary emission efficiency.[16]

Since the anode current is constant, this relationship may be rewritten in terms of logarithms for convenience in working with stellar magnitudes as:

$$\ln F = c - n\beta \ln E_d \tag{7}$$

where $c = \ln(i_a/m)$. The voltages between dynode stages are equal, so the net photomultiplier tube potential, E, is proportional to the dynode voltage, and the expression for the flux becomes:

$$\ln F = k - n\beta \ln E \tag{8}$$

with the constant of proportionality included in the constant k.

Under operating conditions, the total flux incident on the photocathode, F', is composed of the flux from the target, F, the flux due to sky brightness, S, and an equivalent flux due to the dark current, D.

$$F' = F + S + D \tag{9}$$

For convenience, let $\delta = S + D$. The equation for the photometer response thus becomes:

$$\ln (F + \delta) = k - n\beta \ln E \tag{10}$$

For absolute photometric measurements, the constants δ and k would have to be evaluated using a known source having the same spectral energy distribution as the objects to be measured. For relative photometric measurements, however, in which one source is compared directly to another, the reference source, the relationship may be further simplified. Let E_o represent the tube potential with no target in the field, i.e., $F = 0$; then:

$$\ln \delta = k - n\beta \ln E_o \tag{11}$$

and let F_* and E_* represent the flux from the reference source and the corresponding tube potential.

$$\ln (F_* + \delta) = k - n\beta \ln E_* \tag{12}$$

These equations may be rewritten as:

$$\delta = e^k E_o^{-n\beta} \tag{13}$$

and

$$F_* + \delta = e^k E_o^{-n\beta} \tag{14}$$

Eliminating k, one obtains:

$$F_*/\delta = (E_o/E_*)^{n\beta} - 1 \tag{15}$$

A similar relationship can be found between the background tube potential, E_o, and the flux and tube potential for a target, F and E.

$$F/\delta = (E_o/E)^{n\beta} - 1 \tag{16}$$

Dividing Equation 15 into Equation 16, one obtains an expression for the ratio of the flux from the target to the flux from the reference source, the relative spectral reflectivity.

$$\frac{F}{F_*} = \frac{(E_o/E)^{n\beta} - 1}{(E_o/E_*)^{n\beta} - 1} \tag{17}$$

This expression is valid if the light from the target and the reference have the same relative spectral energy distribution. This condition is approached in the comparison of satellite and stellar spectra because of the narrow passband of the spectrometer. Over the 150 Å passband, any variations in the flux from a satellite or star can be assumed to be negligible. The effective spectral distribution incident on the photocathode then becomes the filter passband for both sources.

System Constants. Before Equation 17 can be applied to the experimental data, the constant $n\beta$ and the relation between the photometer signal and the photomultiplier tube potential have to be determined. For a constant flux, Equation 6 may be written as:

$$i_a = c' E_d^{n\beta} \tag{18}$$

or, in terms of the total potential on the tube, as:

$$i_a = c E^{n\beta} \tag{19}$$

Measurements of the anode current versus the tube potential for a constant flux were made, and, using Equation 19, an average value was obtained for $n\beta$ of 8.1 with a standard deviation of 0.3.

The photometer signal is derived by sampling the photomultiplier tube potential with a voltage divider and adding a bias potential. There should, therefore, be a linear relationship between the photomultiplier signal, V, and the tube potential, E.

$$E = a + b\ V \tag{20}$$

To determine the constants, a and b, a series of measurements of the tube potential and corresponding photometer signal for varying fluxes incident on the photocathode were made. The Sweet circuit varied the tube potential to keep the anode current constant. A straight line was least square fitted to the data and the resulting relation is:

$$E = 1446 \text{ volts} - 75.63 \times V \tag{21}$$

where both E and V are in volts.

Computations. Because of the quantity of data to be analyzed, it was decided to automate as much of the data

reduction as possible. The Visicorder records were digitized using a Benson-Lehner Model F OSCAR, an analog chart reader device with a punched-card output. Programs were written to convert the Visicorder records into the photometer voltage signal using the voltage-calibration steps, and to compute then the photomultiplier-tube potential and the incident flux using the equations derived above. Routines were also written for plotting the reduced data with a Calcomp plotter. Copies of these programs are on file at the Aerospace Research Laboratories General Physics Laboratory. The computer used in the data reduction was an IBM 7094.

V. Data Analysis

The spectrometer and the data reduction procedures were first tested on astronomical objects and then applied to the measurement of the spectral reflectivity of artificial satellites. The results of these analyses are presented below.

Astronomical Objects

Stars. To test the self-consistency of the experimental procedures, the spectral distribution of the light from G-type stars was measured and compared. If these stars have the same spectral distribution, the ratio of the flux from one star to that from another should be a constant for all wavelengths. Furthermore, that constant should correspond to the observed difference in the brightness of the two stars.

The results of measurements on 11 October 1970 are summarized in Figure 12. The recorded photometer signal for approximately ten spectrometer scans was averaged for each star and this average signal used in computing the flux ratio (Eqs (21) and (17)). Since the sky brightness observed through the 150-Å bandpass of the spectrometer is within the noise of the dark current signal, the dark current signal was used in determining the background tube potential, E_o. The flux ratio has been computed at 90-Å intervals between 4000 and 7000 Å and plotted in Figure 12 for the indicated star pairs.

The resulting plots indicate that the relative spectral

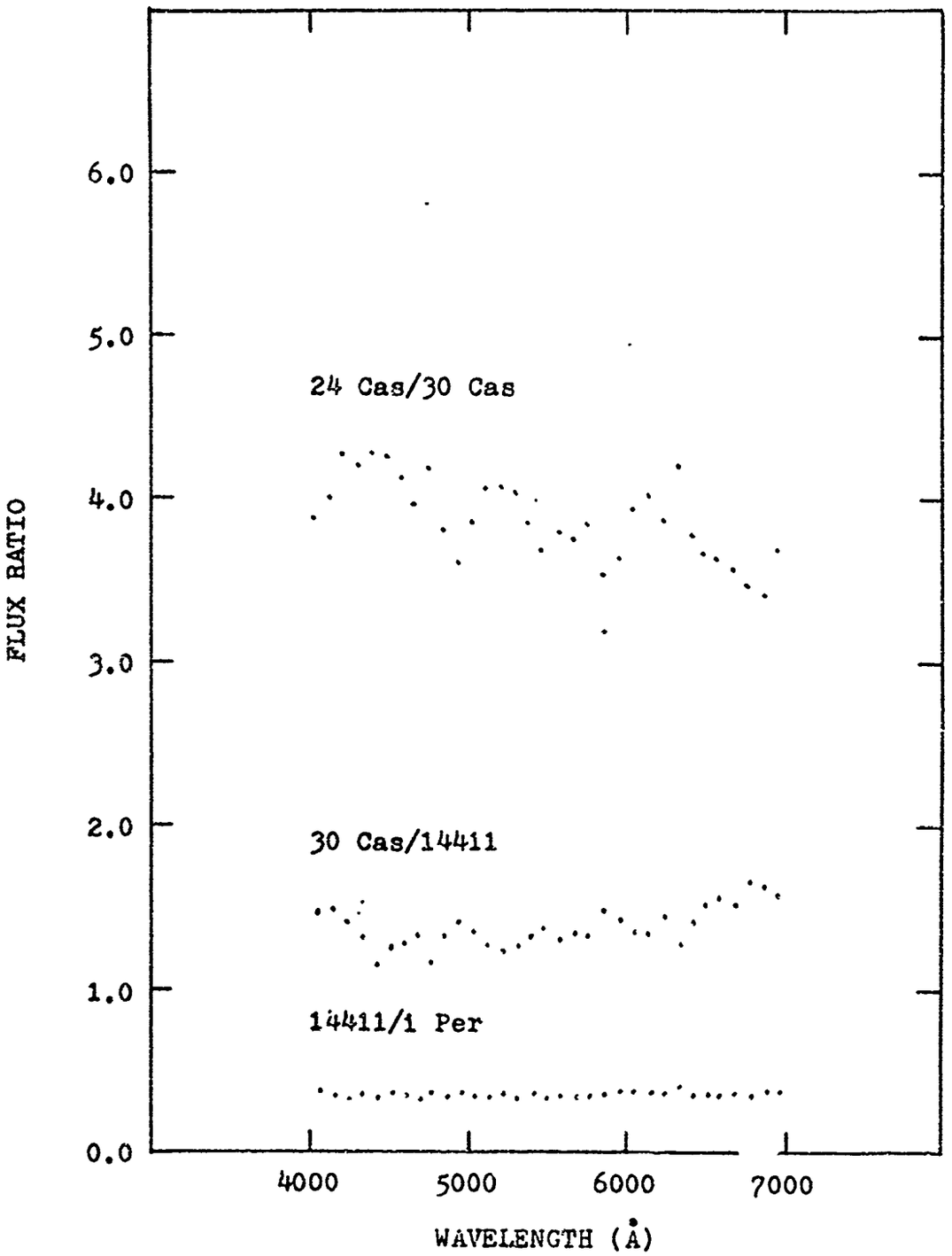

Fig. 12. Comparison of G-Type Stars.

energy distributions are nearly identical. If the distributions had differed significantly, there would have been a pronounced slope in the data points. The multicolor observations of these stars (Table I) are in agreement with this conclusion. It should be noted that the star 30 Cassiopeia is reported to have a peculiar spectrum which could produce some of the observed variations in the flux ratios involving this star. The narrow-band flux ratios for each data set were averaged and the stellar magnitude differences between the stars computed using the definition of the magnitude difference given in Equation 1. The agreement between the magnitude differences (Table III) and those obtained using the visual magnitudes from Table I is good considering that the visual magnitude differences represent a comparison of the integrated fluxes over a much narrower portion of the spectrum.

Table III

Measured Stellar Magnitude Differences

Stars	Averaged Flux Ratio	Magnitude Difference	
		Computed	Published*
24 Cas/30 Cas	3.9 ±0.3	-1.5±0.1	-1.69
30 Cas/14411	1.4 ±0.1	-0.4±0.1	-0.38
14411 /1 Per	0.38±0.03	+1.0±0.1	+1.43

*From Table I.

Moon. The spectral reflectivity of an area in the lunar highlands was determined from measurements on 11 October 1970. As before, an average photometer signal was computed and used in calculating the flux ratio. Six measurements were averaged for the moon and ten for the reference star, Iota Perseus. The ratios have been normalized to unity at 5600 Å and are plotted in Figure 13. Representative errors corresponding to one standard deviation are shown.

Values for the spectral reflectivity of the lunar surface as determined by Barabashev[17] and McCord and Johnson[2] have also been plotted in Figure 9 along with the measured spectral reflectivity of lunar samples returned aboard Apollo 11.[18] Both the McCord and Johnson and the Apollo 11 data are representative of the reflectivity of the lunar maria. The Barabashev measurements are for the lunar highlands. Excellent agreement is obtained between all measurements from 4000 to 6400 Å. Beyond 6400 Å, a sharp increase in the reflectivity of the highlands over the reflectivity of the maria is shown in both the Barabashev and the present measurements.

Artificial Satellites

Object 2253. Object 2253, PAGEOS (Passive Geodetic Earth-Orbiting Satellite), was launched by NASA in 1966 as part of the National Geodetic Satellite Program. PAGEOS is a 100-ft diameter inflated sphere with a surface of vapor-deposited aluminum on a mylar substrate.[19] The satellite

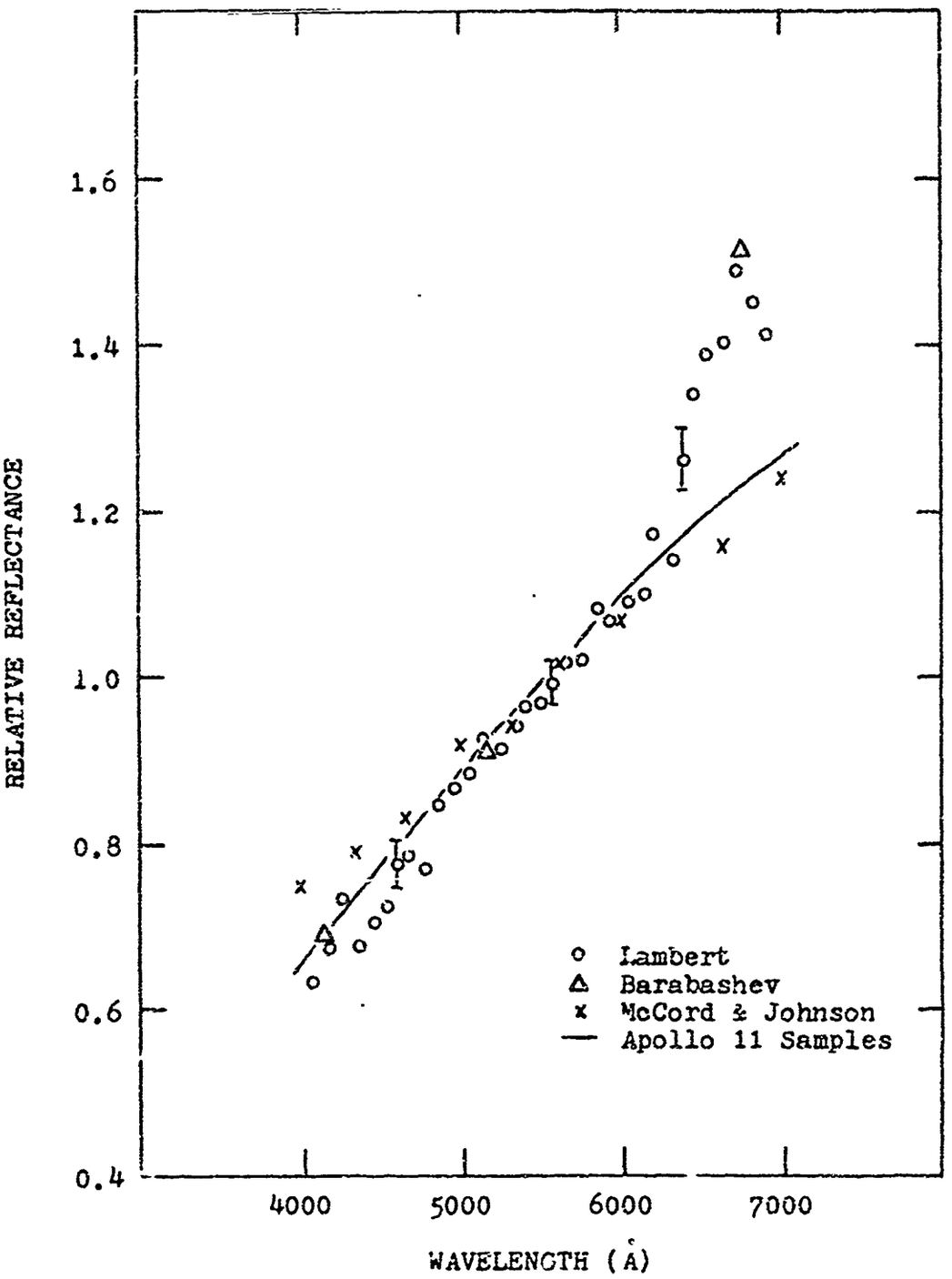

Fig. 13. Lunar Spectral Reflectivity.

is in an orbit with an apogee of 5635 km, and a perigee of 2726 km.[20]

PAGEOS was observed on 7 November 1970. A twenty-second segment of the photometric record over which the brightness of the satellite remained nearly constant was selected for analysis. To compensate for any minor changes in brightness, each spectrometer scan was reduced separately and normalized to unity at 5500 Å. The resulting reflectivity values were averaged, and these averages are plotted in Figure 14. The reference star used in the data reduction was lamda Auriga. The multicolor indices (Table I) indicate that its spectrum is nearly identical to that of the sun.

Also plotted in Figure 14 is the normalized reflectance spectrum of aluminum. Fair agreement is obtained throughout the wavelength region between the experimental points and the aluminum spectrum. The slight skewing of the experimental points is probably the result of either a slight mismatch of the spectrum of the reference star to that of the sun, or a degradation of the aluminum surface.

On this transit, a simultaneous observation was made from the Ohio State University Perkins Observatory, Delaware, Ohio, using a 26-inch objective-prism Schmidt. The dispersion of this system is in declination; so, to avoid having the satellite moving in the direction of the dispersion, it was necessary to make the observation at a point where the apparent trajectory is tangent to a circle of declination.

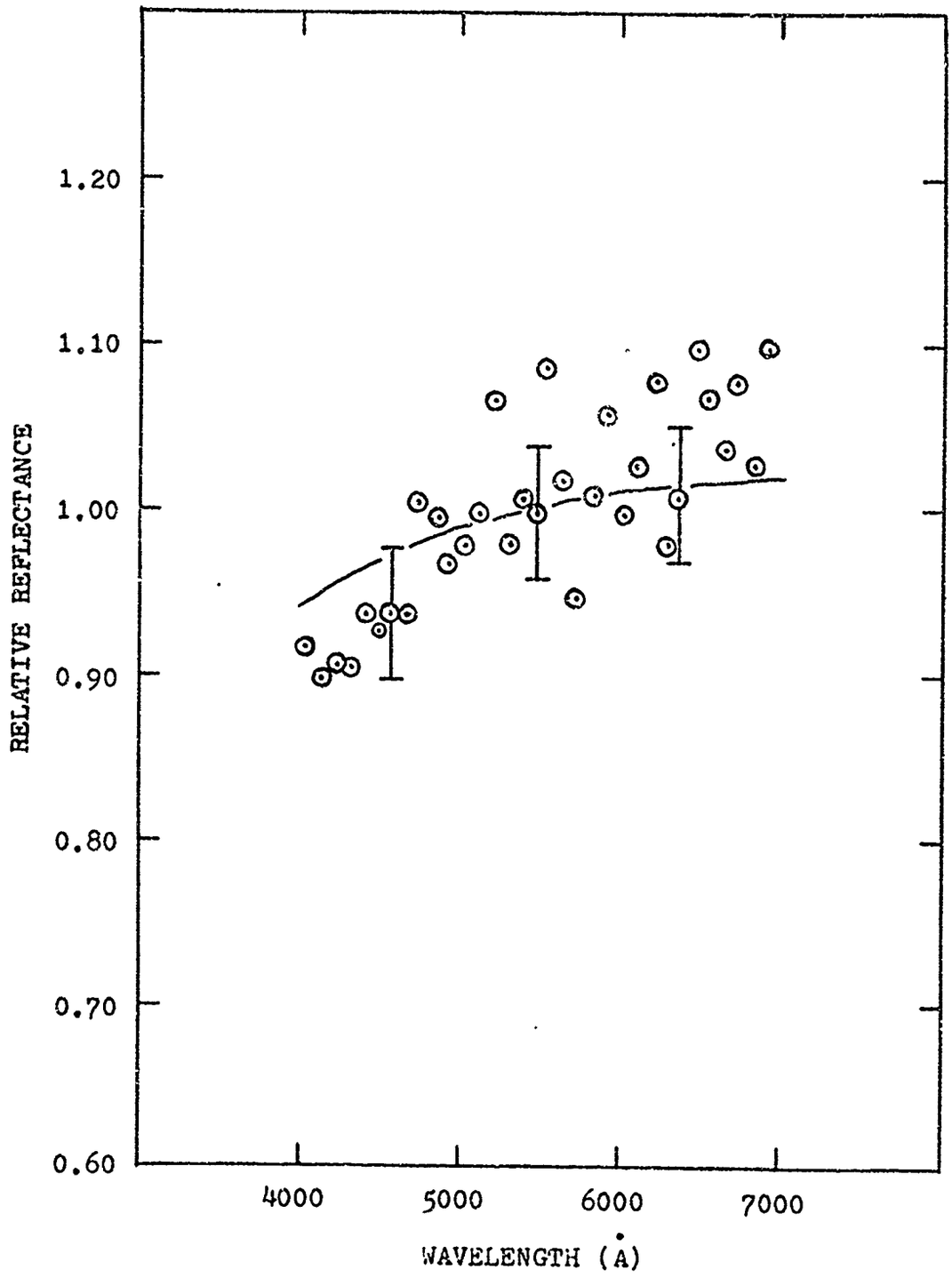

Fig. 14. Object 2253 Reflectance Spectrum. Data is normalized to unity at 5500 Å. Solid line is normalized reflectance spectrum of aluminum.

Following a suggestion by Kissell[21], this point was determined using a modification of the analog technique used in computing the telescope mount settings. The spectral resolution of the Ohio State system is slightly better than that of the spectrometer, so it was hoped to obtain a spectrum for comparison with the photoelectric data. However, even using one of the fastest plates available, the trailed image of PAGEOS was underexposed.

Object 3819. Object 3819 is a Soviet upper stage rocket used in the launching of Cosmos 272 on 17 March 1969. This object is in a nearly circular orbit of radius 1190 km and 73.9° inclination.[20] Photometric observations at Sulphur Grove indicate that this object is tumbling with a period of 110 seconds.

Spectral measurements were obtained for this object on 11 October 1970. The light curve (Fig. 15) is typical of that observed for a tumbling diffuse cylinder, although the sharpness of the peaks indicates that the surface may have some specular characteristics. The brightness on this transit varied between +8 and +4 stellar magnitudes. Spectrometer scans near the light curve maxima were selected for analysis. Because of the uncertainty of the exact shape of the maxima, scans spanning a maxima were not analyzed. Each scan was reduced seperately, then correction applied to compensate for brightness variations during the scan. The correction factors were determined by fitting a straight line to the broadband brightness measurements immediately

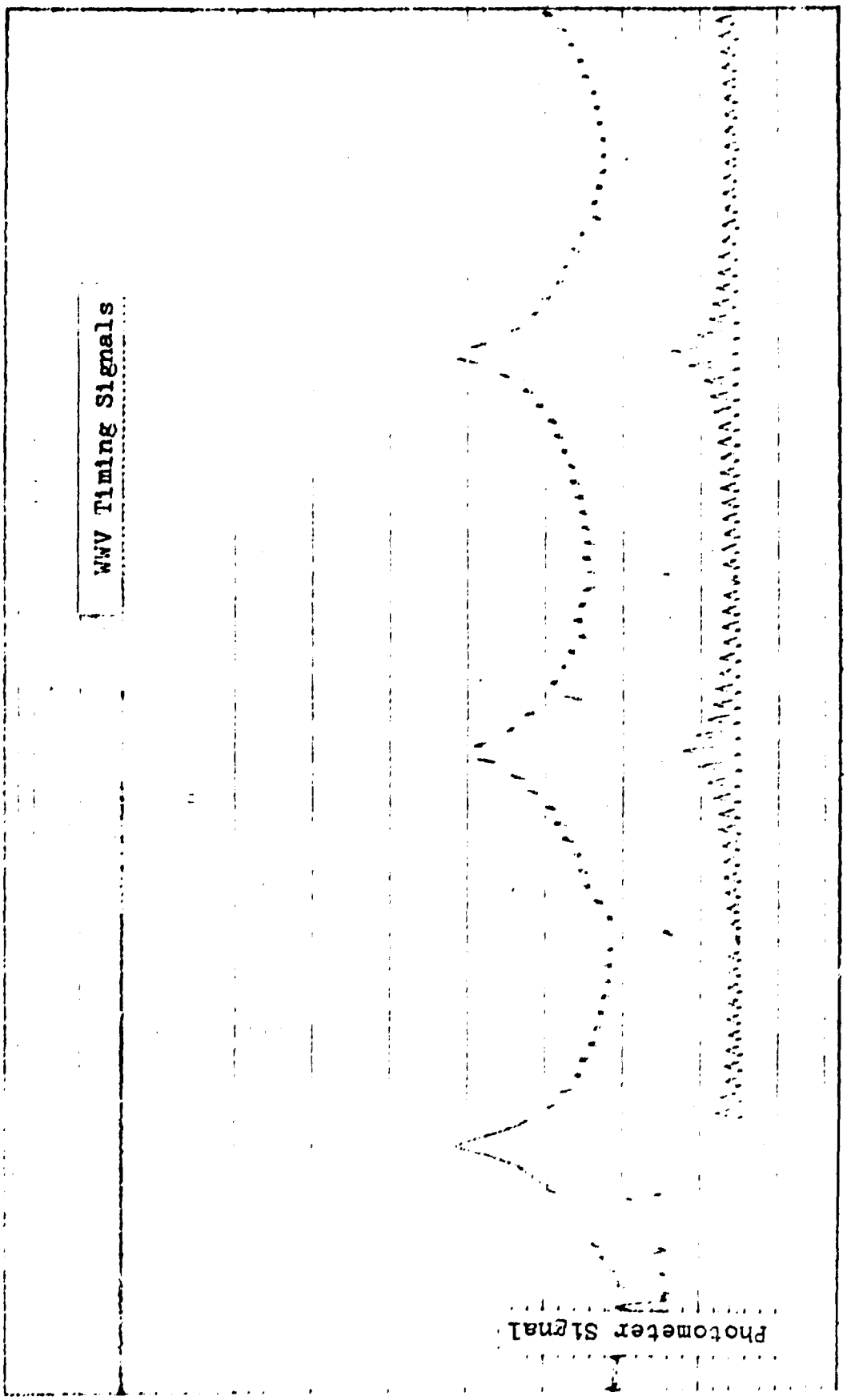

Fig. 15. Object 3819 Light Curve. (11 October 1970)

before and after a scan, and dividing the computed spectral flux ratio at each point by the interpolated broadband flux. The corrected spectral measurements were then averaged. The averages are plotted in Figure 16. The reference star used in the data reduction was iota Perseus. The large uncertainties in the data points may be due in part to errors in the calculated brightness correction factor.

Based on the reflectance spectrum and the broadband observations, it appears that object 3819 is painted with a white, semi-glossy paint. The diffuse scattering with the specular characteristics near the maxima is indicative of a painted surface, and the nearly uniform reflectivity throughout the visible wavelengths indicates a white surface. The decrease in the reflectivity below 4500 Å is typical of zinc-oxide or titanium-dioxide pigments (Fig. 17), both commonly used in white paints. The absorptions at 5100 Å and 5800 Å could permit a more detailed identification of the paint.

Object 4392. Object 4392 is the upper stage of the rocket used to launch the first satellite of the People's Republic of China on 24 April 1970. The orbit of object 4392 has an apogee of 2367 km, a perigee of 441 km, and an inclination of 68.4°.[20]

Spectral observations of this object were made on 8 January 1971. The light curve obtained for this transit (Fig. 18) shows small periodic variations in the brightness indicative of a tumbling diffuse cylinder. Specular glints,

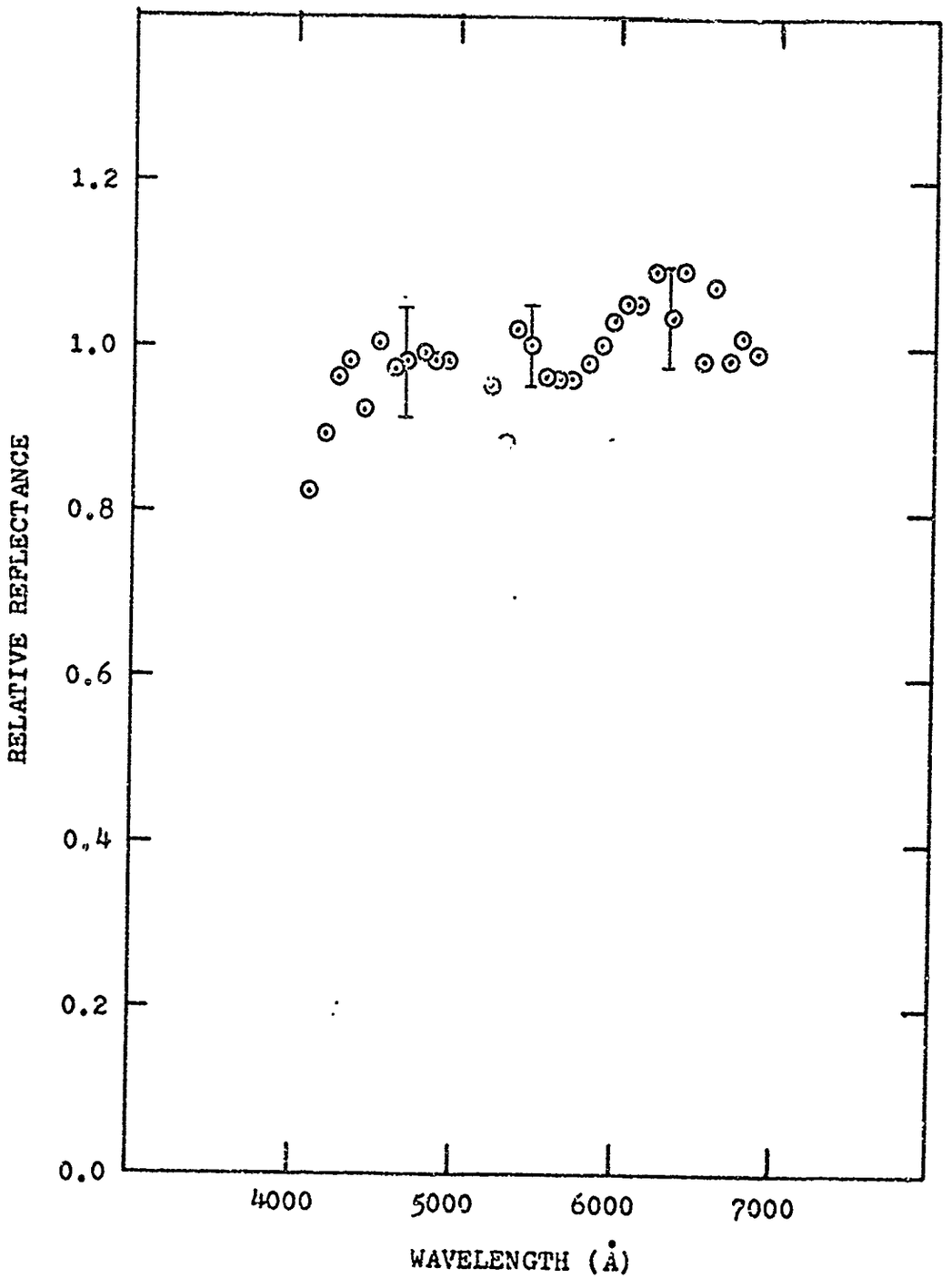

Fig. 16. Object 3819 Reflectance Spectrum. (Normalized to unity at 5500 A.)

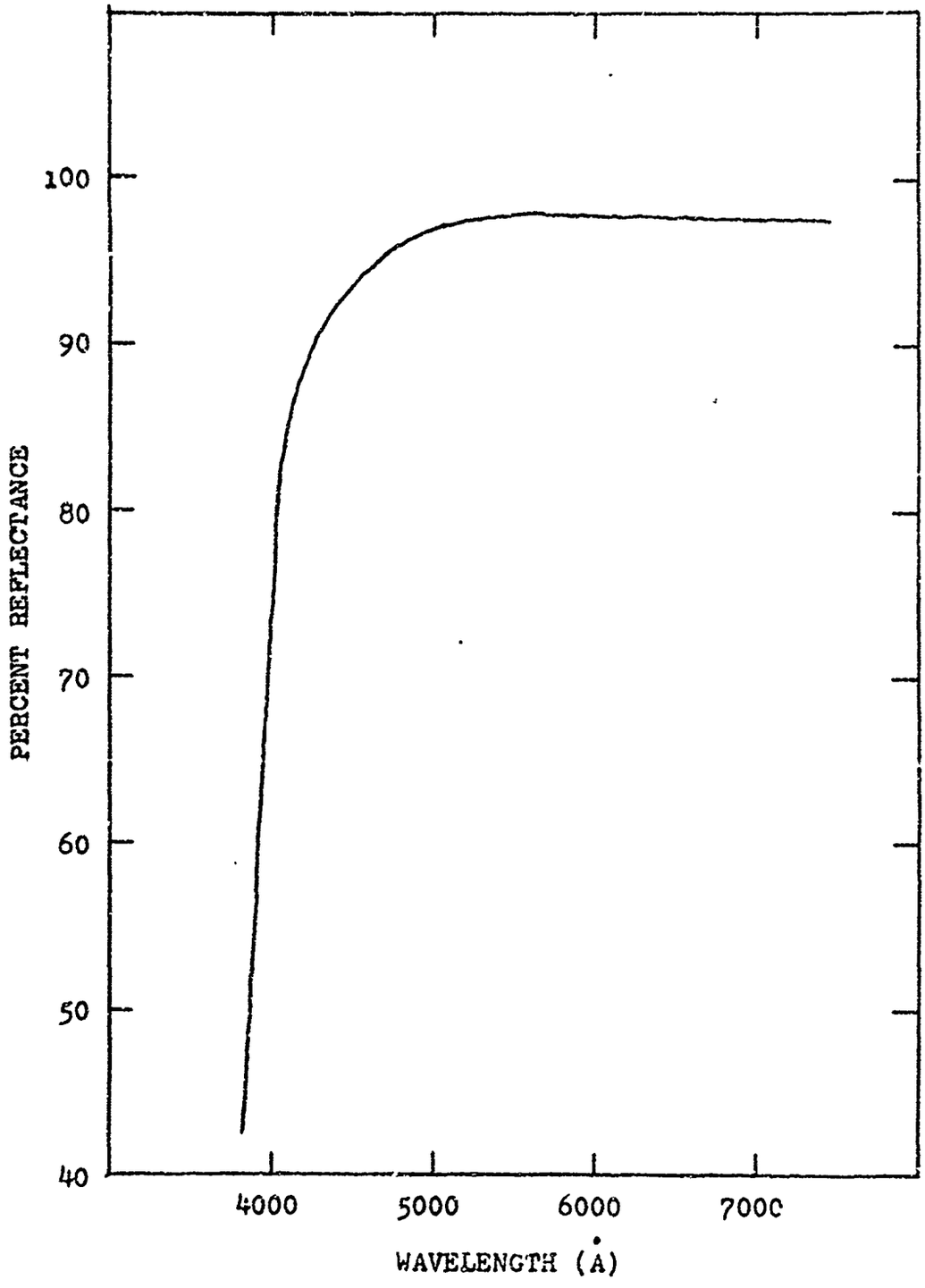

Fig. 17. Reflectance Spectrum of Zinc Oxide.[22]

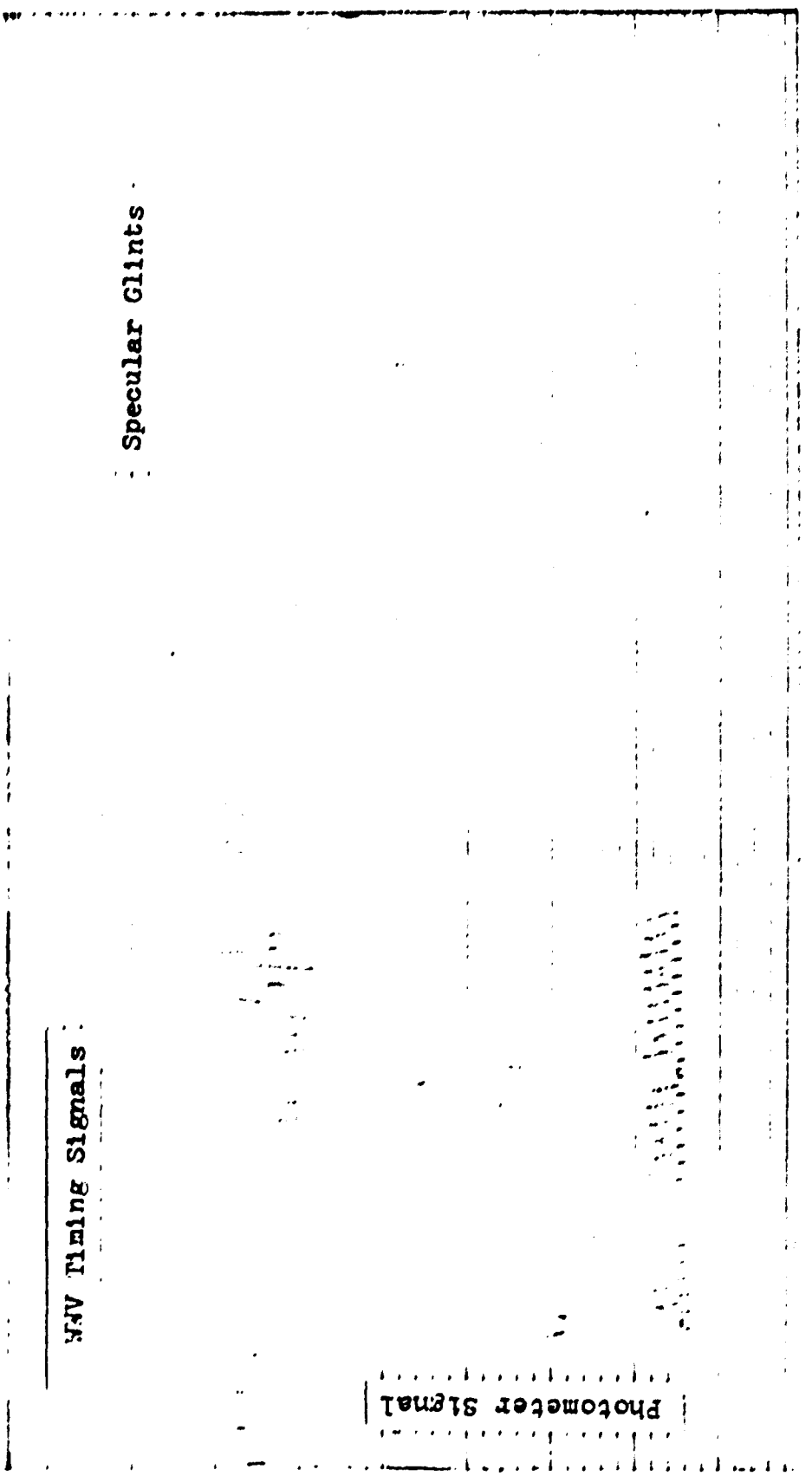

Fig. 18. Object 4392 Light Curve. (8 January 1971)

possibly from some other surface of the satellite are also present. Because the brightness variations were very repeative during the period of observation, interpolation of the broadband flux during the spectral scans was possible by continuing the observed variations across the interval of the spectral scans. The broadband measurements in the scanning cycles were used to check the accuracy of the interpolation.

As for the previous satellite, the interpolated broadband flux was used to correct the computed relative spectral reflectively values for the variations in the satellite brightness. The average corrected values are plotted in Figure 19. The general appearance of the reflectance spectrum of object 4392 is similar to that of object 3819. The reflectivity is nearly uniform throughout the visible wavelengths and decreases in the near ultraviolet. However, the absorptions at 5100 and 5800 Å are absent. The interpretation of the reflectance spectrum of object 4392 is that the surface is covered with a white paint, but of a different type than the paint used on object 3819.

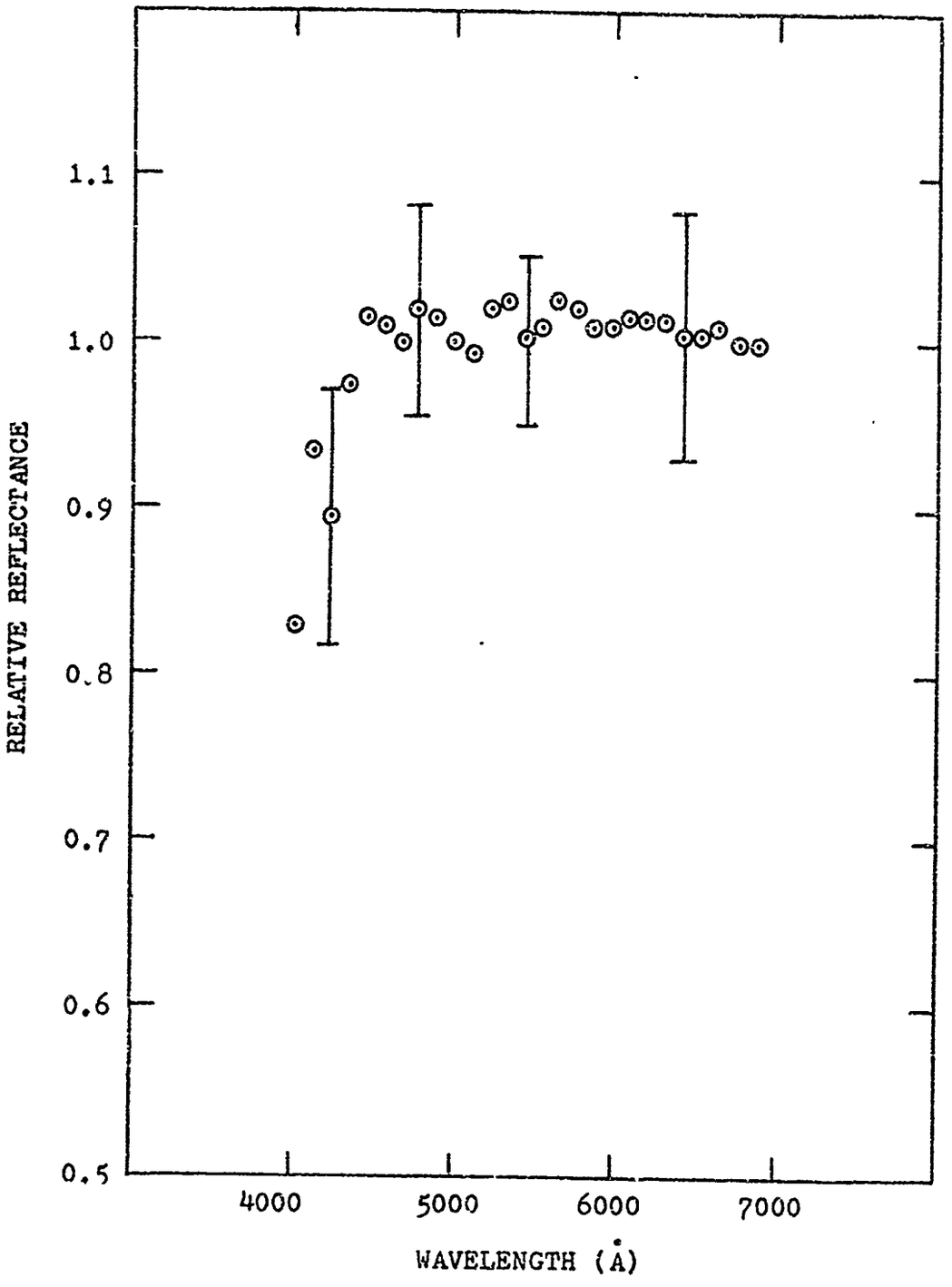

Fig. 19. Object 4392 Reflectance Spectrum. (Normalized to unity at 5500 Å)

VI. Conclusions and Recommendations

Conclusions

This study has demonstrated the feasibility of measuring the low-resolution reflectance spectra of orbiting satellites. A prototype spectrometer was designed and built, and the necessary data reduction procedures developed. The system was successfully tested. Preliminary measurements on orbiting satellites indicate that the reflectance spectra can be used to classify satellite surface materials.

Continued use of the spectrometer at the ARL Sulphur Grove facility is expected. The design is such that it does not interfere with the normal broadband observations at the site. The spectrometer added less than five pounds to the weight of the instrument package previously on the telescope and only 3/4 inch to the overall dimensions. Conversion from spectral to broadband observations consists only of stopping the spectrometer scanning motor at the proper point in the scanning cycle. The simplicity of this conversion has permitted both broadband and spectral observations of a satellite during a single transit.

Recommendations

The spectral reflectivity measurements on satellites should be continued; only a brief beginning was possible in this study. A logical next study would be an intensive study of a single satellite of special interest. By

monitoring the reflectance spectrum over a period of time, any changes in the spectrum due to degradations of the satellite surface by the space environment can be recorded. These degradations have been produced in the laboratory, but the only previous technique for observing changes produced by the actual space environment was by means of on-board experiments.

The techniques developed in this study can be further refined to provide more detailed information on the composition of satellite surfaces. For example, the spectral measurements can be correlated with an analysis of the broadband brightness to determine differences in the reflectance of different areas of a satellite surface. Another area for investigation would be the development of a technique for spectral analysis of specular glints such as are produced by solar cell arrays. The analysis could permit identification of the type of solar cell. More information can be obtained if the spectral measurements are extended further into the ultraviolet. One means of doing this would be to use the second order transmission of the OCLI filter.

The largest approximation made in computing the spectral reflectivity of a satellite was the correction for the changes in brightness. The accuracy of the computations can be greatly improved if the spectrometer is converted to a dual-beam instrument. The broadband brightness of the satellite could be monitored continuously with one beam

while spectral measurements were made in the second beam. The dual-beam system would have the added advantage of permitting measurements of targets with rapid brightness variations. At the present time, measurements are restricted to those objects whose variations are slow in comparison to the spectrometer scanning rate.

In its simplest form, this conversion would consist of replacing the framing camera now on the telescope with a second photometer and using the existing beam splitter to divide the light between the two beams. The outputs of the two photometers could be fed into an analog computer and the ratio of the narrow-band to the broadband flux computed to Equation 17. This ratio divided by a similar ratio for a reference star would yield the relative spectral reflectivity corrected for any brightness variations.

The derived relationships between the flux incident on the photocathode and the photometer signal also have application to the broadband observations at Sulphur Grove. In place of the empirical calibration curves presently used, the stellar calibration data can be fitted to Equation 10:

$$\ln (F + \delta) = k - n\beta \ln E \qquad (10)$$

and an analytic expression obtained for the photometer response. This expression can then be used in the reduction of the photometric light curves with digital computers. An assumption implicit in the use of G-type stars to generate the calibration curves has been that the satellites reflect

the solar spectrum uniformly. The spectrometer can be used to test this assumption and determine its limitations.

Bibliography

1. McCord, T.B., J.B. Adams, and T.V. Johnson. "Asteriod Vesta: Spectral Reflectivity and Compositional Implications." Science, 168: 1445-1447 (19 June 1970).

2. McCord, T.B. and T.V. Johnson. "Lunar Spectral Reflectivity (0.30 to 2.50 Microns) and Implications for Remote Mineralogical Analysis." Science, 169: 855-857 (28 August 1970).

3. Tyson, E.T. "Visual Observations of Several Satellites at the AFAL Cloudcroft Electro-Optical Surveillance Research Facility." Restoration of Atmospherically Degraded Images. Washington: National Academy of Sciences, National Research Council, July 1966.

4. Kissell, K.E. "Diagnosis of Spacecraft Surface Properties and Dynamic Motions by Optical Photometry." Space Research IX. Amsterdam: North-Holland Publishing Company, 1969.

5. Emmons, R.H., C.L. Rogers, and R.J. Preski. The Astronomical Journal, 72: 939 (1967).

6. Lambert, J.V. "Computer Analysis of Photometric Light Curves." Paper presented to: NORSIC 2 (NORAD Space Identification Conference), United States Air Force Academy, Colorado, 1970.

7. Kortum, G. Reflectance Spectroscopy. New York: Springer, 1969.

8. Iriarte, B., H.L. Johnson, R.I. Mitchell, and W.K. Wisniewski. "Five-Color Photometry of Bright Stars." Sky and Telescope, 30: 21-31 (July 1965).

9. Eggen, O.J. "Colors, Luminosities, and Motions of the Nearer G-Type Stars." The Astronomical Journal, 69: 570-609 (October 1964).

10. Kissell, K.E. and R.C. Vanderburgh. Photoelectric Photometry--A Potential Source for Satellite Signatures. ARL 66-0162. Wright-Patterson Air Force Base, Ohio: Aerospace Research Laboratories, 1966.

11. Stead, R.P. An Investigation of Polarization Phenomena Produced by Space Objects. Unpublished Thesis. GSP/PH/67-7. Wright-Patterson Air Force Base, Ohio: Air Force Institute of Technology, 1967.

12. Kissell, K.E. Advantages of a 4-Axis Tracking Mount for the Photoelectric Photometry of Space Vehicles. ARL 65-260. Wright-Patterson Air Force Base, Ohio: Aerospace Research Laboratories, 1965.

13. Lissberger, P.H. and W.L. Wilcock. "Properties of All Dielectric Interference Filters II. Filters in Parallel Beams of Light Incident Obliquely and in Convergent Beams." Journal of the Optical Society of America, 49: 126-130 (February 1959).

14. Vanderburgh, R.C. A Prediction and Tracking Method for Small-Aperture, Continuous Optical Tracking of Artificial Satellites. ARL 66-0008. Wright-Patterson Air Force Base, Ohio: Aerospace Research Laboratories, January 1966.

15. Sweet, M.H. "An Improved Photomultiplier Tube Color Densitometer." Journal of the SMPTE, 54: 35-62 (January 1950).

16. Macknik, L.S. Photoelectric Position Detector for Satellite Tracking. Unpublished Thesis. GSP/PH/69-11. Wright-Patterson Air Force Base, Ohio: Air Force Institute of Technology, 1969.

17. Fressenkov, V.G. "Photometry of the Moon." Physics and Astronomy of the Moon (Z. Kopal, Editor). New York: Academic Press, 1962.

18. Adams, J.B. and R.L. Jones. "Spectral Reflectivity of Lunar Samples." Apollo 11 Lunar Science Conference. Washington: American Association for the Advancement of Science, 1970.

19. "TRW Space Log." Redondo Beach, California: TRW Systems, Summer 1966.

20. National Aeronautics and Space Administration. GSFC Operations Control Center Satellite Situation Report, Vol. 10, No. 6. Greenbelt, Maryland: Office of Public Affairs, Goddard Space Flight Center, 30 September 1970.

21. Kissell, K.E. Personal Communication.

22. Blakemore, J.S. et al. Solar-Radiation-Induced Damage to Optical Properties of ZnO-Type Pigments. NAS 8-11266. Sunnyvale, California: Lockheed Missiles & Space Company, 1965.